Optical properties of urban aerosol from airborne and ground-based in situ measurements performed during the Etude et Simulation de la Qualité de l'air en Ile de France (ESQUIF) program

Patrick Chazette, Hariliva Randriamiarisoa, Joseph Sanak, Pierre Couvert, Cyrille Flamant

Optical properties of urban aerosol from airborne and ground-based in situ measurements performed during the Etude et Simulation de la Qualité de l'air en Ile de France (ESQUIF) program

Patrick Chazette, Hariliva Randriamiarisoa, Joseph Sanak, and Pierre Couvert

Laboratoire des Sciences du Climat et de l'Environnement, Commissariat à l'Energie Atomique, CNRS, Gif-sur-Yvette, France

Cyrille Flamant

Institut Pierre-Simon Laplace, Service d'Aéronomie, CNRS-UPMC, Paris, France

Received 24 March 2004; revised 5 October 2004; accepted 9 November 2004; published 25 January 2005.

[1] Urban aerosol microphysical and optical properties were investigated over the Paris area coupling, for the first time, with dedicated airborne in situ instruments (nephelometer and particle sizers) and active remote sensor (lidar) as well as ground-based in situ instrumentation. The experiment, covering two representative pollution events, was conducted in the framework of the Etude et Simulation de la Qualité de l'air en Ile de France (ESQUIF) program. Pollution plumes were observed under local northerly and southerly synoptic wind conditions on 19 and 31 July 2000, respectively. The 19 July (31 July) event was characterized by north-northwesterly (westerly) advection of polluted (clean) air masses originating from Great Britain (the Atlantic Ocean). The aerosol number size distribution appeared to be composed mainly of two modes in the planetary boundary layer (accumulation and nucleation) and three modes in the surface layer (accumulation, nucleation, and coarse). The characteristics of the size distribution (modal radii and geometric dispersion) were remarkably similar on both days and very coherent with the aerosol optical parameters retrieved from lidar and nephelometer measurements. The city of Paris mainly produces aerosols in the nucleation mode (modal radius of $\sim$0.03 μm) that have little influence on the aerosol optical properties in the visible spectral range. The latter are largely dominated by the scattering properties of aerosols in the accumulation mode (modal radius of $\sim$0.12 μm). When the incoming air mass is already polluted (clear), the aerosol in the accumulation mode is shown to be essentially hydrophobic (hydrophilic) in the outgoing air mass.

Citation: Chazette, P., H. Randriamiarisoa, J. Sanak, P. Couvert, and C. Flamant (2005), Optical properties of urban aerosol from airborne and ground-based in situ measurements performed during the Etude et Simulation de la Qualité de l'air en Ile de France (ESQUIF) program, *J. Geophys. Res.*, *110*, D02206, doi:10.1029/2004JD004810.

1. Introduction

[2] Air quality management in both urban and suburban areas has become a major problem of our modern society over the past twenty years [e.g., *Bennet et al.*, 1985]. Air pollution by aerosols has an impact on regional and global climates [e.g., *Ramanathan et al.*, 2001; *Intergovernmental Panel on Climate Control* (*IPCC*), 2001; *Léon et al.*, 2002; *Sheridan et al.*, 2002] as well as on ecological equilibrium [e.g., *Barker and Tingey*, 1992] and population health [e.g., *Jones*, 1999; *Harrison and Yin*, 2000]. Aerosols do influence gaseous molecules photodissociation [e.g., *Randriamiarisoa et al.*, 2004] and can thus have significant impact on the photo-oxidant pollution [e.g., *Dickerson et al.*, 1997].

0148-0227/05/2004JD004810

[3] Automobile traffic is the main source of photo-oxidant pollution and aerosols in large cities such as Paris (France) [e.g., *Menut et al.*, 2000], Los Angeles (California) [e.g., *Lurmann et al.*, 1997] or Athens (Greece) [e.g., *Durieux et al.*, 1998; *Eleftheriadis et al.*, 1998]. The nonlinear character of chemical transformations occurring during the aerosol aging processes makes it difficult to set up regulation policies for aerosol emissions. Aerosols can either be directly emitted or formed by gas-to-particle conversion. Their chemical composition can evolve through interaction with clouds or by condensation of organic volatile compounds and/or by reacting with water vapor [e.g., *Forstner et al.*, 1997].

[4] Because little was known about the size distribution of the anthropogenic aerosols in the Paris area and their optical properties, an intensive 2-year field campaign was carried out in the framework of the Etude et Simulation de la Qualité de l'air en Ile de France (ESQUIF) program. Its

aim was to better understand the processes leading to air pollution peaks in Paris by combining experimental and modeling approaches [*Menut et al.*, 2000; *Vautard et al.*, 2003a]. The ESQUIF program lasted from July 1998 to July 2000. Results concerning the photo-oxidant pollution have been well documented in the special section "Atmospheric Pollution Over the Paris Area (ESQUIF)" in *Journal of Geophysical Research* [e.g., *Vautard et al.*, 2003b; *Beekmann and Derognat*, 2003; *Derognat et al.*, 2003] but a description of the aerosol characteristics had yet to be done. Measurements were mainly performed during the summer to document the photochemical processes leading to ozone peaks. Prior the summer of 2000 some aerosol measurements were performed but the data were too scarce to enable a relevant assessment of the aerosol properties around Paris.

[5] The main experiment devoted to aerosols trapped in the planetary boundary layer (PBL) was scheduled during the last two Intensive Observation Periods (IOPs) of ESQUIF, between 17 and 31 July 2000. During these IOPs, instruments devoted to aerosol measurements were simultaneously operated onboard an aircraft and in a ground-based mobile experimental station. Other studies on aerosol optical properties were previously conducted using airborne measurements such as during the Tropospheric Aerosol Radiative Forcing Observational Experiment (TARFOX) [e.g., *Russel et al.*, 1999] off the East coast of United States, the Second Aerosol Characterization Experiment (ACE 2) [e.g., *Carrico et al.*, 2000] off the coast of Portugal, or the Indian Ocean Experiment (INDOEX) [e.g., *Pelon et al.*, 2002] off the west coast of India. The Lindenberg Aerosol Characterization Experiment (LACE 98) combined in situ measurements with aircraft and lidars over highly populated area (southeast of Berlin, Germany) [*Ansmann et al.*, 2002]. Lidars were also used in the framework of the European Aerosol Research Lidar Network (EARLINET) to establish an aerosol climatology and define a quantitative comprehensive statistical database of both horizontal and vertical distribution of aerosols on a continental scale [*Matthias et al.*, 2004]. Nevertheless, these campaigns, except LACE 98, did not use simultaneous in situ and backscatter lidar measurements performed both from aircraft to retrieve aerosol optical properties and size number concentration. Furthermore, they were not conducted over an urban center of more than 12 millions inhabitants such as the Paris area.

2. Experimental Setup

2.1. Instruments

[6] To characterize aerosols over the Paris area, we have used two main instrumental platforms: a mobile station (MAS, mobile aerosol station) for surface in situ measurements in the suburban areas and the French research aircraft Fokker27/ARAT (Avion de Recherche Atmosphérique et de Télédétection) for in situ and remote sensing measurements within the lower troposphere. The aircraft instrumentation included the lidar LEANDRE-1 (Lidar aéroporté pour l'Etude des Aérosols, des Nuages, de la Dynamique, du Rayonnement et du cycle de l'Eau), two nephelometers and an optical particle sizer. The aerosol sampling was performed through an isokinetic probe located, in the free air stream, on the right forepart of the Fokker 27 fuselage. This isokinetic sampler, commercialized by GeoSens B.V. (Rotterdam) and validated for the study of submicron aerosol onboard airplanes, has been well described by *Pena et al.* [1977]. The flow rate, for each instrument sampling line, is controlled to ensure flow conditions as close as possible to isokinetism. Other measurements such as ozone (O_3), nitrogen monoxide (NO) and carbon monoxide (CO) were also recorded and used as tracers of polluted air masses. The aircraft velocity was $\sim$90 m s^{-1} and data were acquired with a temporal sampling rate of 1 second. The MAS equipment included a particle counter, two optical particle sizers, a nephelometer and a Sun photometer. Data acquisition was performed at a temporal sampling rate of 1 minute. The MAS positioning within the Paris suburbs and the aircraft flight plans were determined according to air masses synoptic motions. Atmospheric state parameters (pressure, temperature, relative humidity and wind vector) were also monitored on both instrumental platforms.

2.1.1. Lidar LEANDRE1

[7] The ARAT was equipped with the backscatter lidar LEANDRE 1 to document the atmospheric reflectivity at 532 nm and 1064 nm in the lower troposphere. These lidar measurements were the first ever made from an airborne platform over the Paris area.

[8] LEANDRE 1 uses submicron aerosols as tracers to document the lower tropospheric structure with vertical and horizontal resolutions of 15 and 150 m, respectively [*Flamant and Pelon*, 1996; *Pelon et al.*, 2002]. The lidar signal depends on particle concentration, number size distribution and chemical composition. Thus lidar-derived atmospheric backscattering is generally observed to be large in the atmospheric boundary layer and in elevated aerosol layers inside the free troposphere (residual aerosol or dust aerosol layers). In the present study we use vertical profiles of aerosol extinction coefficient derived from lidar. The different sources of uncertainty are well described by *Chazette et al.* [1995]. The mean relative error for the extinction coefficient is generally less than 10% when the inversion of lidar profiles is constrained using a Sun photometer [e.g., *Chazette*, 2003] and when the relative humidity stays lower than 75%, as is the case here.

2.1.2. Particle Sizers

[9] The airborne optical particle sizer PCASP model 100, developed by Particle Measuring Systems (PMS Inc, Boulder, Colorado), gives access to 15 classes of particles ranging from >0.1 up to >3 μm in diameter. It is used to retrieve the aerosol number size distribution in the lower troposphere. The accuracy on the aerosol number concentration measurement is about 5% for submicron aerosols [*Dye and Baumgardner*, 1984].

[10] In the MAS station, two complementary types of optical particle sizers were used: KC18 (RION Co, Ltd. Japon) and MetOne 237 (http://www.metone.com). The KC18 gives access to the partition function of the aerosol in 5 diameter classes (>0.10 μm, >0.15 μm, >0.20 μm, >0.30 μm, >0.50 μm). The light source is a He-Ne laser at 663 nm and the measurement is performed at 90° scattering angle. The inlet air flow rate is 0.30 L/mn. The MetOne instrument gives the aerosol partition function in 5 diameter classes (>0.30 μm, >0.50 μm, >0.70 μm, >1.00 μm, >2.00 μm, >3.00 μm) and uses a diode laser source, with an inlet flow rate of 2.83 L/mn. Both KC18 and MetOne

instruments were used to retrieve the aerosol number size distribution at the surface level.

2.1.3. Particle/Soot Absorption Photometer (PSAP)

[11] A proxy for black carbon concentration (BC) was retrieved from measurements performed continuously with a PSAP (Radiance Research, Seattle, USA) onboard the ARAT. This instrument is sensitive to the light-absorbing part of the aerosols [*Hansen and Novakov*, 1990] and its measurements are representative of air masses affected by anthropogenic pollution [*Penner*, 1995].

2.1.4. Condensation Particle Counter (CPC)

[12] Number concentrations of submicron particles were measured, onboard the aircraft and the mobile station, with 3022A CPC TSI® model particle counters. These counters detect all particles within a diameter size range from 0.007 to 3 μm, with a 100% efficiency for 0.02 μm. Particle concentrations are retrieved with a relative uncertainty of 5% [*Chazette and Liousse*, 2001].

2.1.5. Nephelometers

[13] Two nephelometers were installed onboard the ARAT: a three-wavelength (450, 550 and 700 nm) nephelometer (manufactured by TSI®) and a mono-wavelength (550 nm) nephelometer (MRI® integrating nephelometer model 1550B). A second monowavelength nephelometer was used in the MAS. These instruments measure the aerosol scattering coefficient in a 7–170° range of scattering angle [e.g., *Bodhaine et al.*, 1991; *Flamant et al.*, 2000]. To take into account the non observed scattering angles, a correction factor ξ has been assessed, from Mie computations, to be close to 1.035, for urban aerosols. This assessment was done using the retrieved aerosol mean size number distribution (see section 3.2) and the mean complex refractive index during July 2000 (see section 4.1). The monowavelength nephelometers were used in ambient relative humidity without heating whereas the three-wavelength instrument scattering chamber was maintained at about 35–40% relative humidity (dry aerosol conditions). The mean relative uncertainty of these instruments is considered to be less than 10% [e.g., *Bodhaine et al.*, 1991] and is mainly due to the variability of the relative humidity inside the instrument. In dry conditions, the relative uncertainty after calibration is around a few per cent (evaluated from the reproducibility of laboratory measurements).

2.1.6. Sun Photometer

[14] The CIMEL® Sun photometer instrument performs integrated measurements of solar light absorption to retrieved aerosol optical properties (optical thickness and complex refractive index, at several wavelengths, and Angström exponent). The channels used for this study are centered at 440 nm and 670 nm, with bandwidths of less than 20 nm. The instrument field of view is about 1° [e.g., *Holben et al.*, 1998]. Optical thickness data of the Paris area were obtained from the Aerosol Robotic Network (AERONET), the MAS Sun photometer being one of its temporary stations. The AERONET database gives a maximal absolute uncertainty of 0.02 for the optical thickness, independent of the aerosol loading. The complex refractive index retrieval, following *Dubovik et al.* [2001], can be obtained for aerosol optical thicknesses larger than 0.3 at 440 nm and is associated with an absolute error of 0.04 for the real part and a relative uncertainty of about 30% for the imaginary part. The uncertainty on the Angström exponent has been shown to be ~0.03 for aerosol optical thickness of ~0.2 [*Hamonou et al.*, 1999].

2.2. Synoptic Conditions and Airborne Operations

[15] Only two pollution events (19 and 31 July 2000) were explored through airborne measurements because of flight restrictions over Paris and rather poor weather conditions. For the first event, Paris was under the influence of a north-northwesterly synoptic flow, with noticeable amount of scattered cumulus and air masses coming from over Great Britain, as illustrated by the back trajectories computed over 3 days and ending over Paris on 19 July at 1200 UTC (Figure 1, top). For the second event, the synoptic circulation changed and Paris was under the influence of a westerly air flow. The 3-day back trajectories show that the air mass advecting over Paris on 31 July was coming from the Atlantic Ocean. The westerly flow coming from the ocean was advected east of Paris before being recirculated clockwise, entering the Paris area from the south (Figure 1, bottom) as confirmed from airborne wind measurements (see section 2.3).

[16] A statistical analysis of summertime air masses origins has been performed using the NOAA HYSPLIT4 Model [*Draxler and Hess*, 1998]. A sample of 455 five-day back trajectories ending over Paris (900 m MSL) at 1200 UTC were computed for June, July, and August for the years 1999–2003. This analysis shows that 45% of the back trajectories originated directly from the Atlantic Ocean (as on 31 July) and 17% of them passed over the industrialized areas of the Great Britain (as on 19 July). These situations were the two most representative during the summers of this 5 year period.

[17] Flight plans were established according to the daily synoptic conditions and PBL depths using ECMWF (European Center for Medium-range Weather Forecast) forecasts and the flight altitudes imposed by Air Traffic Control. In situ measurements of aerosol microphysical and optical properties were performed at a flight altitude of ~900 m above mean sea level (MSL) within the PBL and nadir pointing lidar measurements were made from an altitude of ~4200 m MSL in the free troposphere. Flight plans for both 19 and 31 July, together with the raw aerosol scattering coefficient measured by the airborne nephelometer, are shown in Figures 2a and 2b and illustrate the location of the pollution plume around Paris.

[18] The major difference between the two periods was the direction of the air flow. To better sample the urban pollution production, crosswind flight legs were performed within the PBL, one upwind and at least two downwind of Paris. On 19 July, under northerly wind conditions, two flights were performed at 1040–1330 UTC and 1420–1715 UTC. The first flight started from Creil with a low-level upwind leg (L1) before climbing to 4200 m MSL for two legs north (T1) and south (T2) of Paris. The aircraft then descended to perform two downwind legs (L2, L3) at 900 m MSL before landing at the Vatry airport, ~140 km east of Paris. After refueling, the aircraft headed back west to sample legs L2 and L3 again, as well as a third leg (L4) further south over the countryside. The end of this flight was devoted to lidar measurements with a first crosswind leg (T3) coinciding with L4 and then a south-north segment

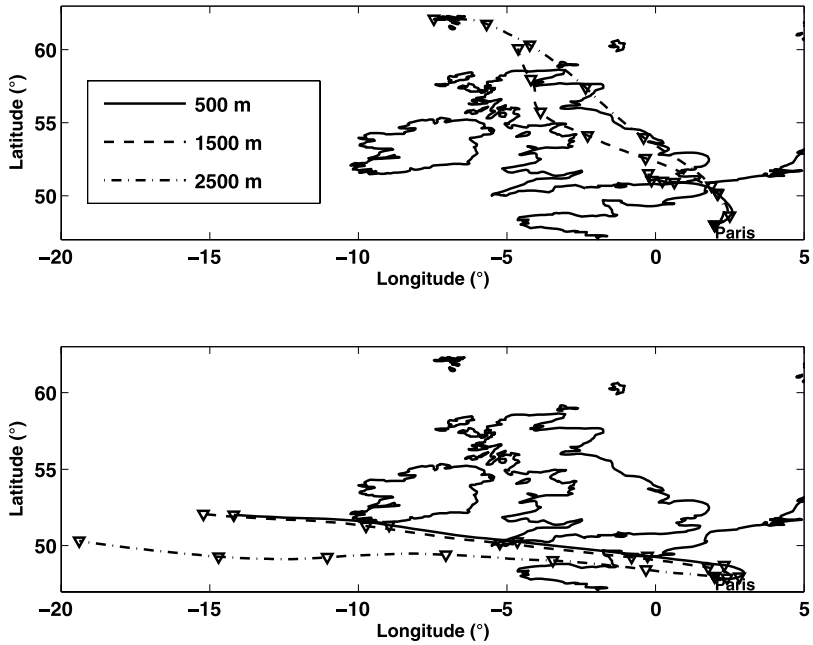

Figure 1. Back trajectories for two 3-day periods ending over Paris at 1200 UTC on (top) 19 July and (bottom) 31 July at 0.5, 1.5, and 2.5 km MSL (courtesy of NOAA Air Resources Laboratory http://www.arl.noaa.gov). The triangles give the 12-h spacing.

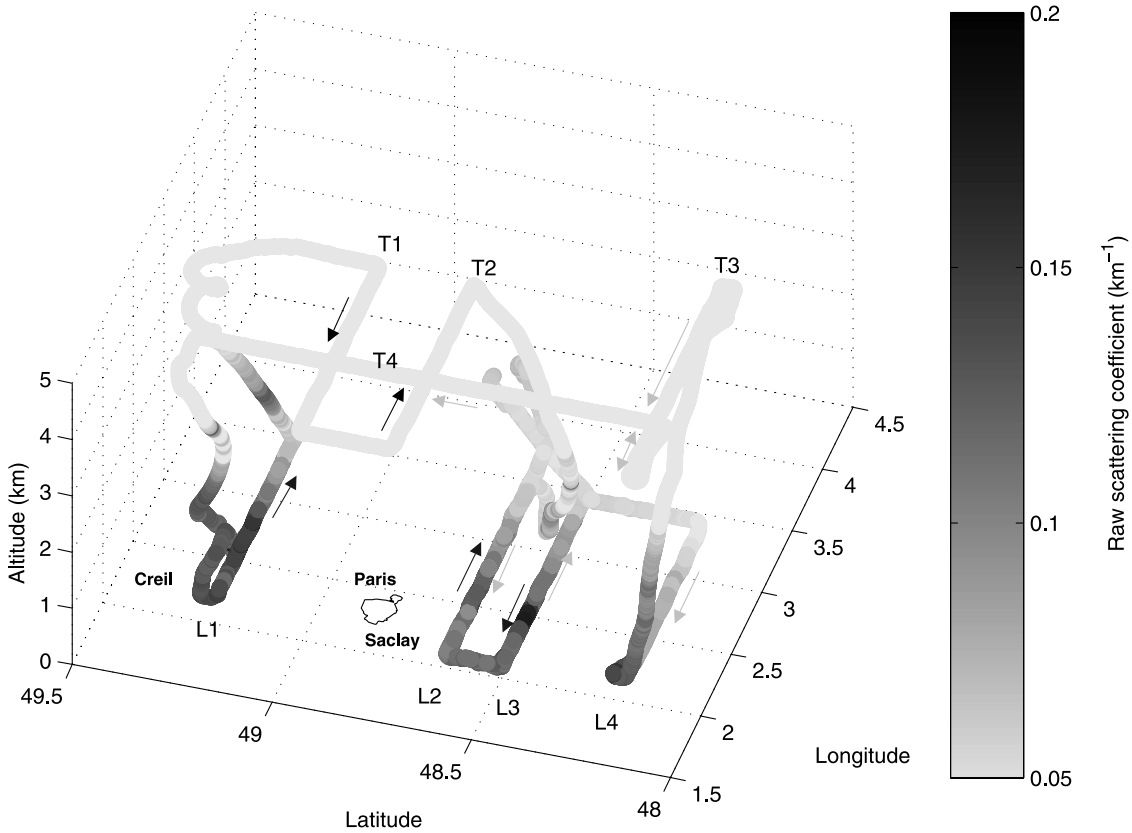

Figure 2a. Flight plans for 19 July 2000. In situ aerosol measurements in the PBL were performed at ~900 m (labeled Li) and lidar measurements were performed at ~4200 m MSL (labeled Ti). The direction of flight is indicated by arrows. The solid and shaded arrows refer to the first and second flights, respectively (see text for details). The raw scattering coefficient measured onboard the aircraft is color coded (only the second flight is given for legs L2 and L3).

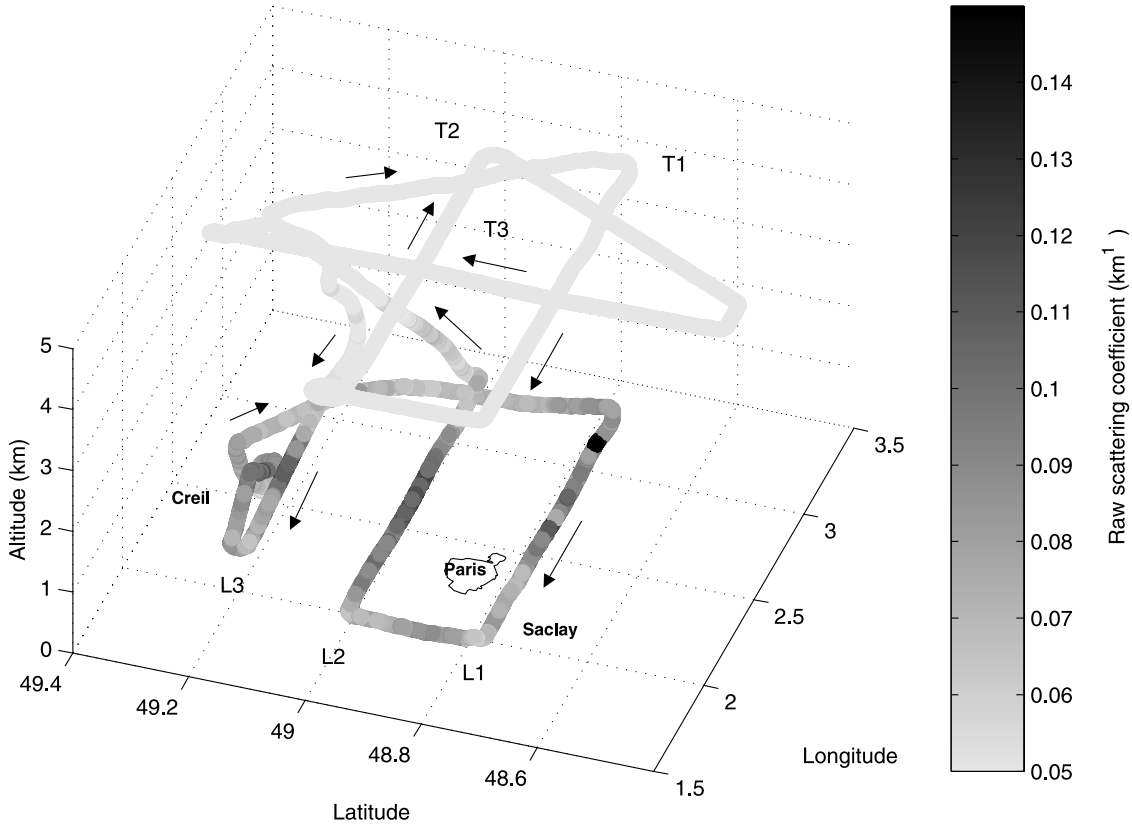

Figure 2b. Flight plans for 31 July 2000. In situ aerosol measurements in the PBL were performed at ~900 m (labeled Li) and lidar measurements were performed at ~4200 m MSL (labeled Ti). The direction of flight is indicated by arrows. The raw scattering coefficient measured onboard the aircraft is color coded.

(T4) toward Creil. On 31 July the flight was scheduled between 1030 and 1400 UTC. From Creil, the aircraft headed south at 900 m MSL and performed an upwind leg (L1) and a downwind leg (L2) before climbing to 4200 m MSL at which height lidar measurements were made on two legs, T1 and T2, colocalized respectively with L1 and L2. The flight ended with a south-north oriented leg devoted to lidar measurements (T3) and a third low-level aerosol sampling leg (L3) downwind of Paris. While flying at 900 m MSL, the aircraft always remained within the PBL.

[19] On 19 July the upwind leg was performed 36 km north of the city, over the countryside, whereas the downwind legs where performed at 35, 50, and 85 km from Paris. On 31 July, the upwind leg was flown over a rather urbanized area, about 12 km south of center Paris, while the downwind legs were flown 11 and 36 km north of Paris.

2.3. Air Masses Characterization

[20] Besides the difference in air mass origins, the back trajectories, shown in Figure 1, highlight different air circulations around the Paris area. Aircraft wind speed and direction (Figure 3) measurements confirm these synoptic trends. On 19 July, the air mass entered over Paris from the north with a mean wind speed of 7 m s^{-1} in the PBL. According to the virtual potential temperature and relative humidity profiles, the mean PBL depth was about 1600 ± 200 m during the entire flight period. On 31 July the air mass entered the Paris area from the south with a mean wind speed of 3 m s^{-1}. The PBL depth was then about 1700 ± 200 m. These PBL depths are confirmed by backscatter lidar profiles (see sections 3 and 4).

[21] Tropospheric ozone is a good tracer of urban pollution and its concentration is recorded at ground level on a continuous basis by the AIRPARIF (http://www.airparif.assoc.fr) network. On 19 July the ozone concentration increased between 1400 and 1500 UTC from 65 ppbv in Cergy (30 km northwest of Paris) to 70 ppbv in Les Ulis (25 km southwest of Paris). Such an increase is within the instrumental error and thus not significant. This means that the air mass arriving over Paris was already ozone-rich as reported by *Vautard et al.* [2001] during a previous ESQUIF case study observed in the summer of 1998. For 31 July a significant increase was observed, with ozone concentrations of 48 ppbv in Les Ulis and 80 ppbv in Cergy. This suggests that the air mass was cleaner upstream and that the production of ozone precursors by the Paris area was non negligible. These trends are confirmed by the airborne ozone measurements (not shown).

[22] Sun photometer observations give further insight on the air masses atmospheric quality. For 19 July the retrieved optical thicknesses at 550 nm were 0.25 ± 0.03 before 1030 UTC and 0.3 ± 0.05 before 1200 UTC above Palaiseau and Paris respectively. After these hours, no other reliable optical thicknesses data were available due to increased

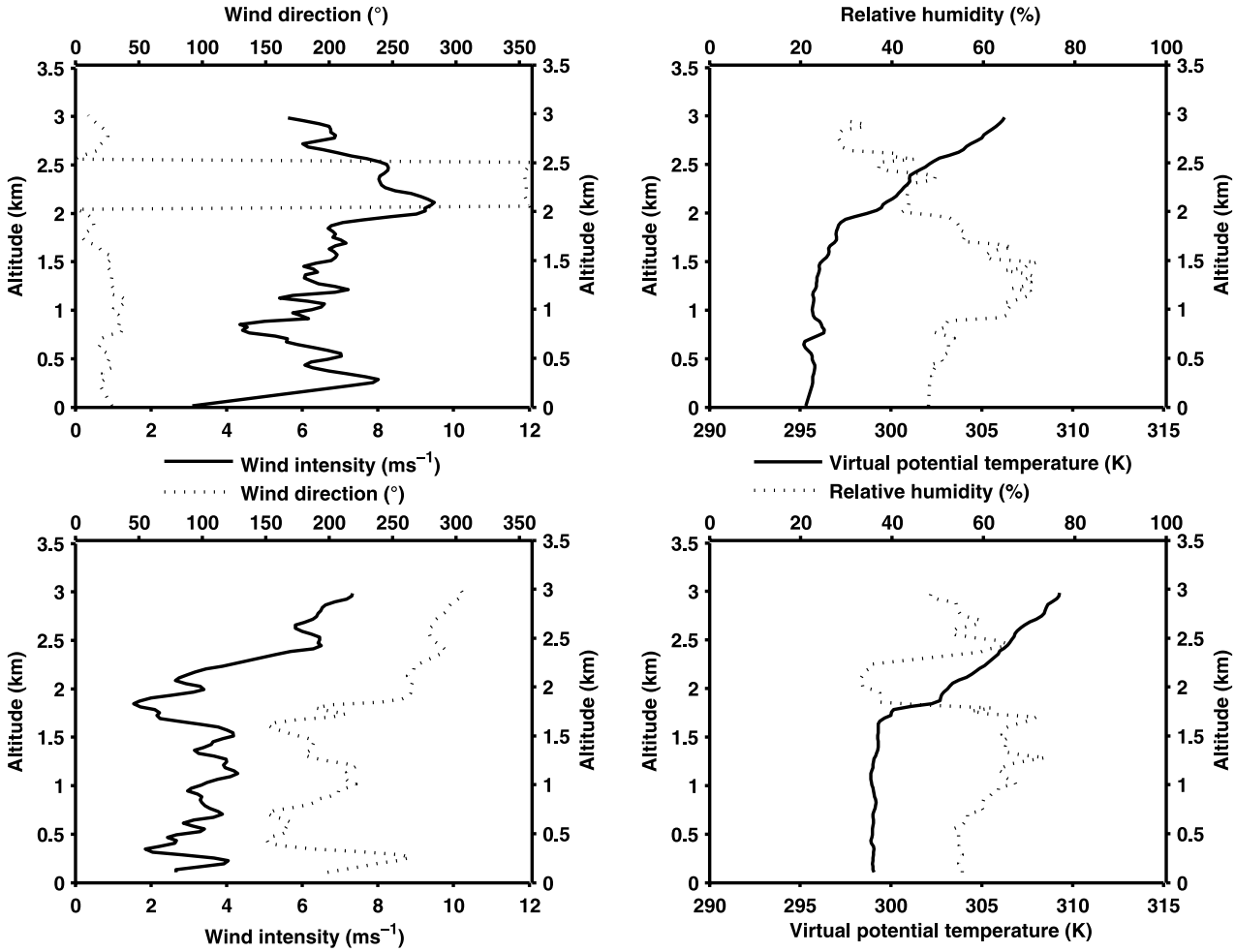

Figure 3. Profiles of (left) wind intensity and direction and (right) virtual potential temperature and relative humidity for (top) 19 July and (bottom) 31 July acquired onboard the ARAT in the vicinity of Creil shortly before landing. The soundings were obtained around 1330 and 1400 UTC on 19 and 31 July, respectively.

cloudiness. For 31 July the mean optical thicknesses were smaller with values of 0.11 ± 0.03 above Palaiseau or Creteil (respectively south and southeast of Paris), 0.15 ± 0.03 above Paris and 0.22 ± 0.04 above Creil (North of Paris), but pointing out a significant increase downwind of the urban area. The given standard deviations take into account both the error on the optical thickness retrieval and the temporal measurement variability. These observations are compatible with the ozone measurements trends. Figure 4 shows the occurrences of the total optical thickness at 550 nm over the Paris area during the years of 1999 and 2000, in clear-sky conditions, as obtained from Sun photometer measurements performed at Créteil, Palaiseau, and Paris (AERONET network [*Holben et al.*, 1998]). The two days involved in this experiment are clearly representative of the aerosol loading over Paris.

[23] We are thus in presence of two contrasted, but representative, situations in terms of atmospheric synoptic flows and air quality. On 19 July the advected air mass was already polluted because of its transit over Great Britain and northern France, while on 31 July the incoming rather clean oceanic air mass better underlines the influence of the Paris area urban pollution.

3. Aerosol Size Distribution Retrievals

3.1. Method

[24] A standard method was used to retrieve the aerosol size distributions at 900 m MSL in the PBL, assuming 3 modes (nucleation, accumulation, and coarse) in a lognormal distribution. This method, using the proximity recognition approach [e.g., *Chedin and Scott*, 1985; *Chazette et al.*, 1998], is widely used in geophysical data analysis. A lookup table has been calculated for different lognormal aerosol models in each size class measured by the aerosol sizers. The measured data are then compared to the lookup table to extract the size distribution parameters.

3.2. Size Number Distribution Results

[25] The aerosol size distribution retrievals were obtained after application of a median filter based on a moving window over 21 individual size distribution points. This

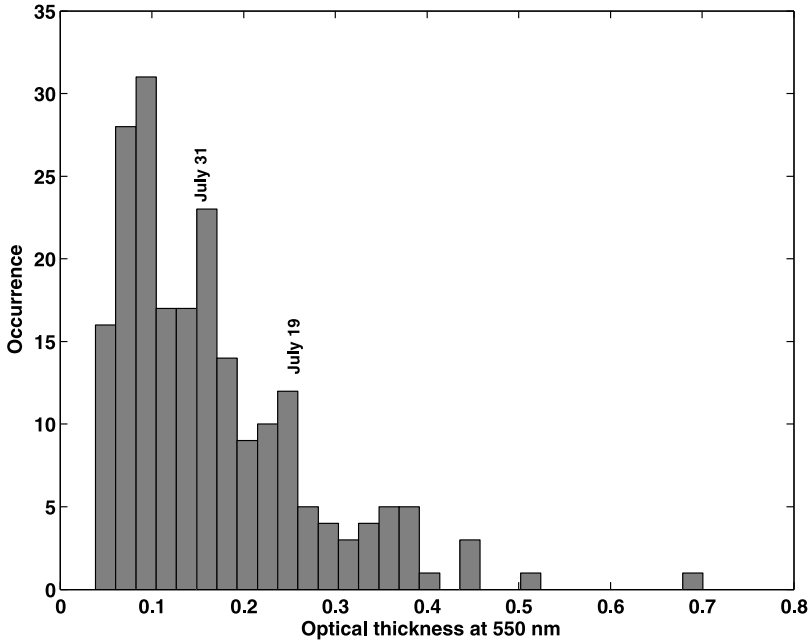

Figure 4. Occurrences of the 550 nm optical thickness for clear-sky conditions during the years 1999 and 2000 in the Paris area. The mean values of the present study for 19 and 31 July 2000 are indicated.

filtering leads to a temporal resolution of ~15 s (horizontal resolution of ~1300 m given the aircraft speed). A bimodal size distribution was determined during both flights and the contribution of a coarse mode was not observed. This may be due to the limited capabilities of the instruments onboard the aircraft because of the isokinetic characteristic of the air inlet and the problem of aerosol impacts inside the sampling lines. Moreover, the onboard particle sizers could present important measurement errors for particles with diameter >0.8 μm [*Cutten et al.*, 1998]. To evaluate such effects, measurements at low altitude, 90 m above the ground level, were performed close to the MAS position on 31 July where independent ground level size distributions were recorded. This was the lowest possible altitude due to the required airplane security regulations. Differences of the order of 10 to 15% have been observed for each class of particles for mean radii smaller than 0.25 μm. The differences for the larger particles were more important, pointing out the difficulty to retrieve the coarse mode from airborne data. Figure 5 shows that above 500 m MSL within the PBL the raw aerosol size distribution varies weakly with altitude. The uncertainties associated with the proximity recognition approach on the retrieved bimodal size distribution parameters have been assessed (see Table 1) using a Monte Carlo approach [*Chazette et al.*, 2001] taking into account the uncertainties due to the PCASP instrument. The comparison of the retrieved bimodal distributions with the direct measurements leads to relative errors lower than 5% as illustrated in Figure 6. Nevertheless it is also necessary to consider the instrumental uncertainty. For aerosol diameters <0.8 μm, the measurement error is close to 5% [*Dye and Baumgardner*, 1984; *Cutten et al.*, 1998]. If the uncertainty sources are considered to be independent, the total error is <10%.

[26] Hereafter, only the 900 m MSL flight legs results are presented and discussed because they correspond to horizontal leveled flight legs where the isokinetic sampler is used according to constructor recommendations [*Pena et al.*, 1977]. The bimodal aerosol size distribution is characterized by the modal radius (r_1) and the dispersion (σ_1) of the first mode (nucleation mode), the modal radius (r_2) and the dispersion (σ_2) of the second mode (accumulation mode) and the occupation rate of the second mode (x_2). The characteristics of the aerosol number size distribution are given in Table 1. Apart from x_2, all the variables characterizing the aerosol size distribution did not change significantly inside or outside of the plume, upwind or downwind of Paris. The occupation rate of the second mode (x_2) is thus used as a proxy of polluted air masses. This choice is also consistent with the fact that aerosols generally grow in size while being transported, and hence large values of x_2 are representative of aged aerosol plumes.

3.2.1. Flights of 19 July

[27] Figure 7 shows that on 19 July the incoming air mass was already rich in aged aerosol indicating that the air mass had flown over polluted areas prior to reaching the Paris area, as suggested in section 2.3. x_2 was not observed to vary significantly within the plume downwind of Paris. Aircraft measurements in the PBL evidenced that the easternmost extension of the plume was located around 2.8°E. x_2 was observed to vary significantly across that boundary, from 30% to less than 15%. The position of the eastern boundary of the plume was confirmed by lidar measurements given in Figure 8 where a significant decrease of both the extinction coefficient and the optical thickness (from 0.25 to 0.15 at 532 nm) is observed east of 2.8°E. The lidar two-dimensional profile shown in Figure 8 was acquired on leg T2 about 10 km downwind (south) of

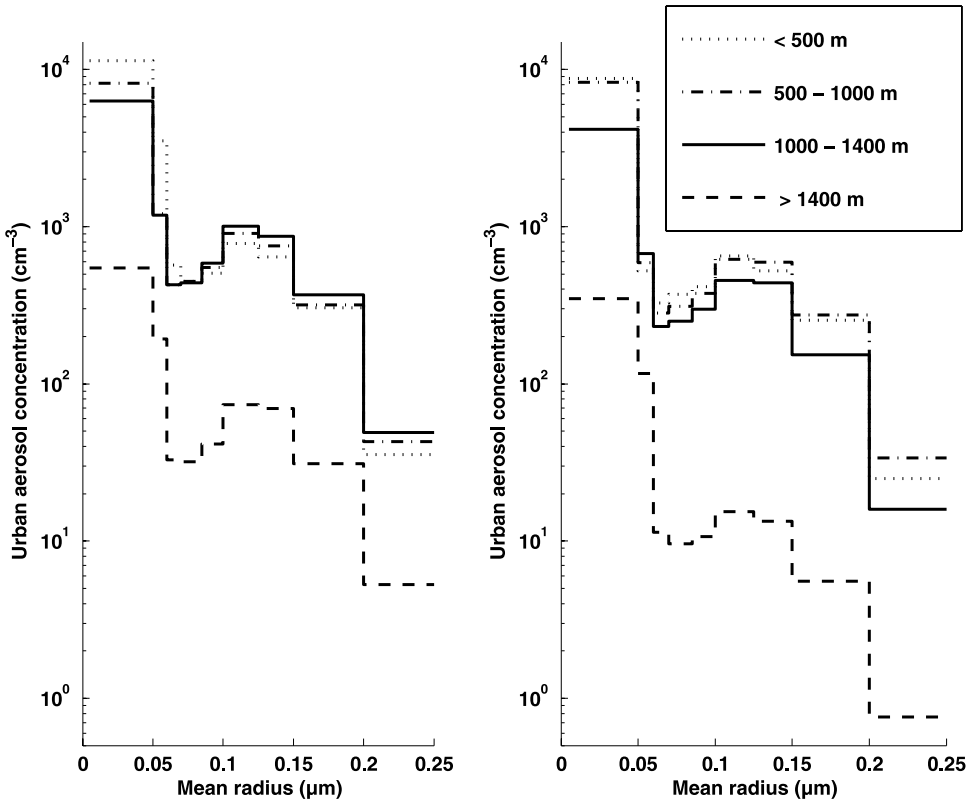

Figure 5. Raw aerosol size distributions measured from aircraft at different altitudes on (left) 19 July and (right) 31 July. These distributions were compiled from all the measurements performed at the different heights mentioned during each flight.

Paris. More details are given about the lidar analysis and its interpretation in the next sections.

3.2.2. Flights of 31 July

[28] Figure 9 shows the evolution of x_2 in the PBL on 31 July. Four regions can be identified: 1) a region of large x_2 values (greater than 22%, domain labeled 1) around Coulommiers, 2) a region of small x_2 values (less than 15%, domain labeled 2) downwind of the Charles de Gaulle Airport, 3) a region around Paris (both up and downwind as seen on legs L1 and L2) where values of x_2 between 15 and 22% are observed, and 4) a region north of Paris (downwind, on leg L3) where values of x_2 are larger than on legs L1 and L2, and are comprised between 17% and 24%. The x_2 values upstream of Paris (leg L1) are lower than those observed upstream on 19 July, consistent with the advection of a less polluted air mass over Paris on 31 July. In Figure 9, no clear signature of the Paris plume can be seen when comparing x_2 values measured on legs L1 and L2. Leg L1 was performed over an already urbanized area and thus the measurements are likely to not be representative of the incoming clean oceanic air mass. Further downstream (Leg L3), the larger values are an indication of the aging of the aerosol. The large x_2 values over the Coulommiers region are thought to be the result of particle

Table 1. Mean Aerosol Size Number Distribution Characteristics Derived From Aircraft and MAS Measurements on 19 and 31 July 2000[a]

	r_1, μm	σ_1	x_1, %	r_2, μm	σ_2	x_2, %	r_3, μm	σ_3
19 July								
Aircraft	0.04 (±0.007)	1.5 (±0.15)	79 (±7)	0.12 (±0.005)	1.3 (±0.05)	21 (±7)	-	-
Saclay	0.03 (±0.01)	1.5 (±0.1)	83.48 (±9)	0.08 (±0.01)	1.5 (±0.1)	16.471 (±6)	0.45 (±0.05)	1.2 (±0.2)
31 July								
Aircraft	0.03 (±0.006)	1.5 (±0.11)	81 (±4)	0.12 (±0.005)	1.3 (±0.04)	19 (±4)	-	-
Creil	0.03 (±0.01)	1.5 (±0.2)	88.77 (±3)	0.08 (±0.01)	1.5 (±0.1)	11.152 (±5)	0.40 (±0.1)	1.3 (±0.1)
Uncertainties from Monte Carlo method	±0.01	±0.01	±3	±0.015	±0.02	±3	±0.1	±0.02

[a]A lognormal size distribution is assumed, which is characterized by up to three modal radii (r_1, r_2, and r_3), the associated geometric dispersions (σ_1, σ_2, and σ_3), and occupation rates (x_1 and x_2). An assessment of the temporal variability is given in parenthesis. The uncertainties due to the retrieval procedure are also specified.

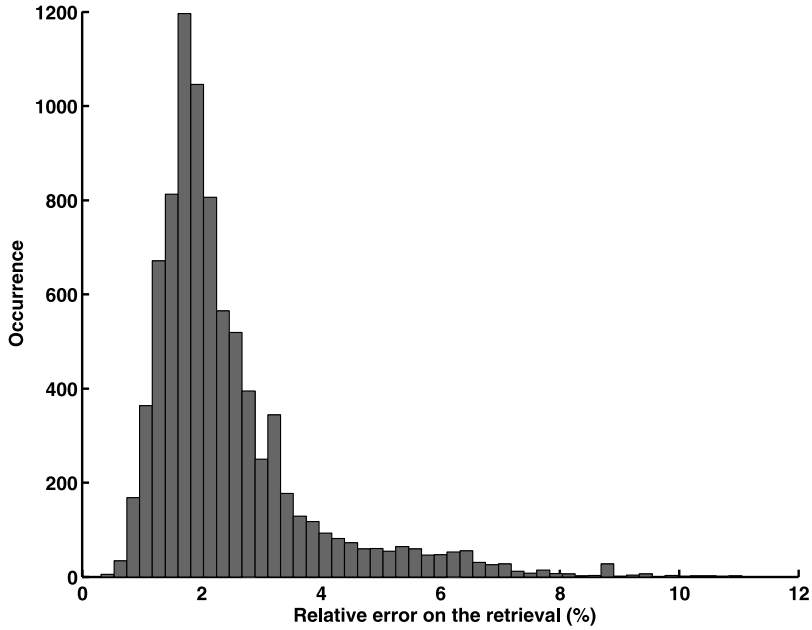

Figure 6. Cumulative occurrences of the relative error on the retrieval of aerosols size distributions from airborne PCASP for the flights of 19 and 31 July 2000.

uptakes in connection with intensive agricultural activity. Note that this region presents a weaker aerosol number concentration ($\sim$4000 cm^{-3}) when compared with the center of the pollution plume ($\sim$10000 cm^{-3}). Such high x_2 values were not observed on 19 July in this region. We hypothesize that this is due to rainfall on the previous days. It rained in this region on 18 July, whereas no rainfall was observed for several days prior to 31 July. The influence of

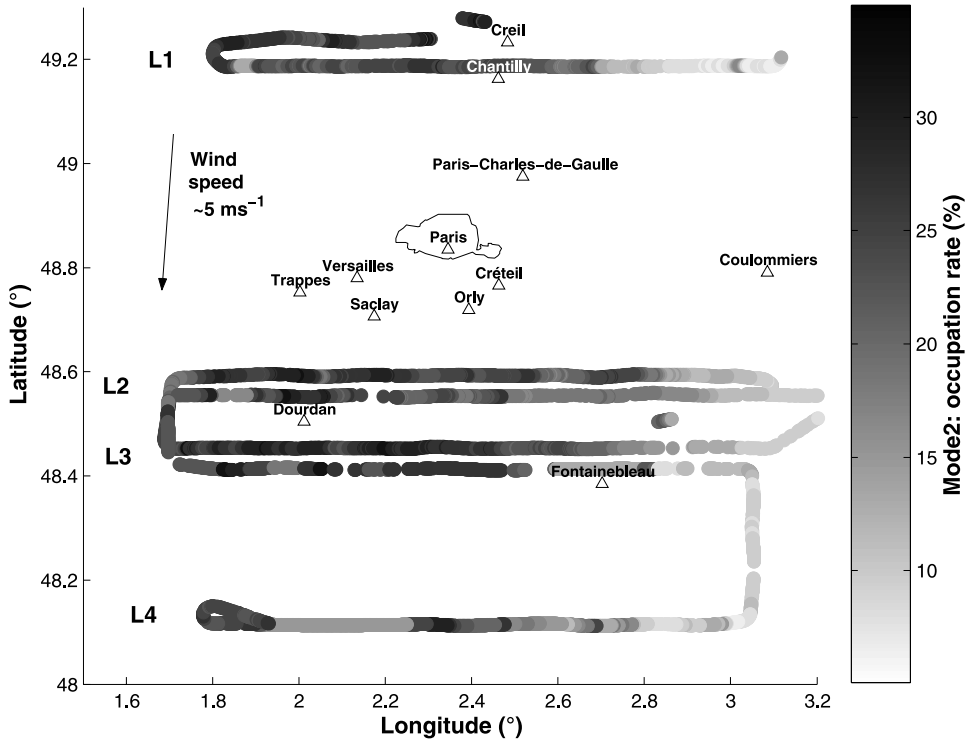

Figure 7. Occupation rate of the second mode (x_2) in the PBL (900 m MSL) along the flight track on 19 July 2000. Legs L2 and L3 for the second flight have been shifted north by 0.04° for the sake of clarity. See color version of this figure at back of this issue.

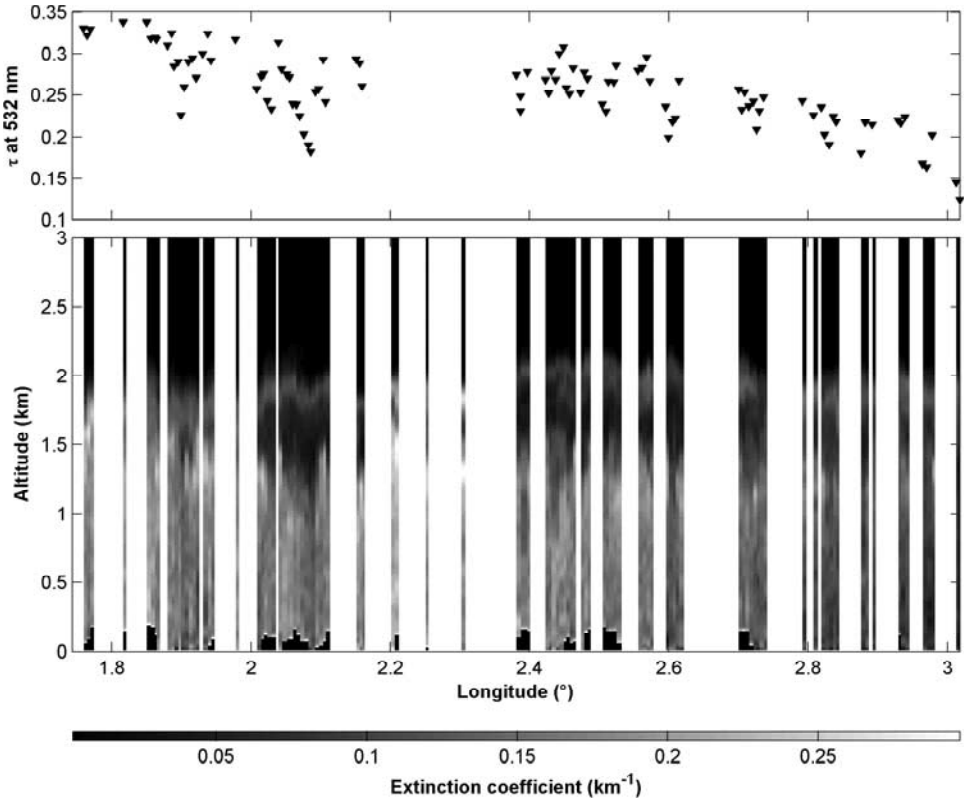

Figure 8. (top) Lidar-derived aerosol optical thickness at 532 nm and (bottom) vertical profile of the extinction coefficient obtained along leg T2 by LEANDRE on 19 July. The vertical white stripes correspond to missing data due to contamination by cumulus clouds present at the top of the PBL.

Charles de Gaulle Airport is clearly observed in Figure 9. The decrease of x_2 values in domain 2 is linked to aircraft emissions that are mainly composed of small particles.

[29] To refine our analysis of the Parisian plume structure for 31 July, we have used airborne measurements of a proxy for black carbon (BC) concentration (i.e., uncalibrated BC concentration in arbitrary units) around Paris (Figure 10). BC is a good tracer of the automobile traffic emissions and further help to situate the aerosol plume. Figure 10 shows a significant increase in BC proxy concentration from upwind to downwind of Paris. On leg L2, the plume is seen between 1.9°E and 2.7°E. The signature of the Parisian plume is also seen on leg L3, west of 2.5°E. The regions around Coulommiers and downwind of Charles de Gaulle Airport do not generate BC, which is why the Parisian plume can be identified unambiguously.

3.2.3. Coherence With Surface Measurements

[30] As a complement of this analysis of the airborne measurements, the size distribution characteristics retrieved from the MAS station ground level measurements, performed downwind of Paris, are shown in Table 1. Given the retrieval method uncertainties and the temporal variability in the measurements, the mean values of the first two modes characteristics can be considered to be essentially the same as those retrieved from aircraft measurements. The main observed differences on the smaller modal radius and the larger occupation rate of the nucleation mode, may point out the proximity of the particle sources within the surface layer. Even if we take into account the uncertainty due to the retrieval method (0.015), the difference between r_2 determined in the mixed layer (0.12 ± 0.005) and at the surface (0.08 ± 0.01) is barely within the error bars. However, this latter low value is probably affected by the large uncertainties on the third mode radius retrieval. Despite an occupation rate of less than 10^{-3}, this coarse mode is identified with modal radii between 0.4 and 0.45 μm.

4. Coherence With Airborne Optical Measurements

[31] This section examines the coherence between the retrieved size number distributions and the optical measurements performed during the same flights.

4.1. Coherence With Nephelometer and Sun Photometer Measurements

[32] To perform calculations of the aerosol optical properties, one needs to know the complex refractive index of these aerosols during the measurement period. The only available estimates of the aerosol refractive index for the time and location of this experiment are those given on the Web site of the AERONET network [*Holben et al.*, 1998]. The average complex refractive index, over the entire month of July 2000, was calculated to be $(1.5 \pm 0.05) - i\,(0.016 \pm 0.0125)$ at 670 nm, after rejection of aberrant data with refractive indices close to that of water. The standard

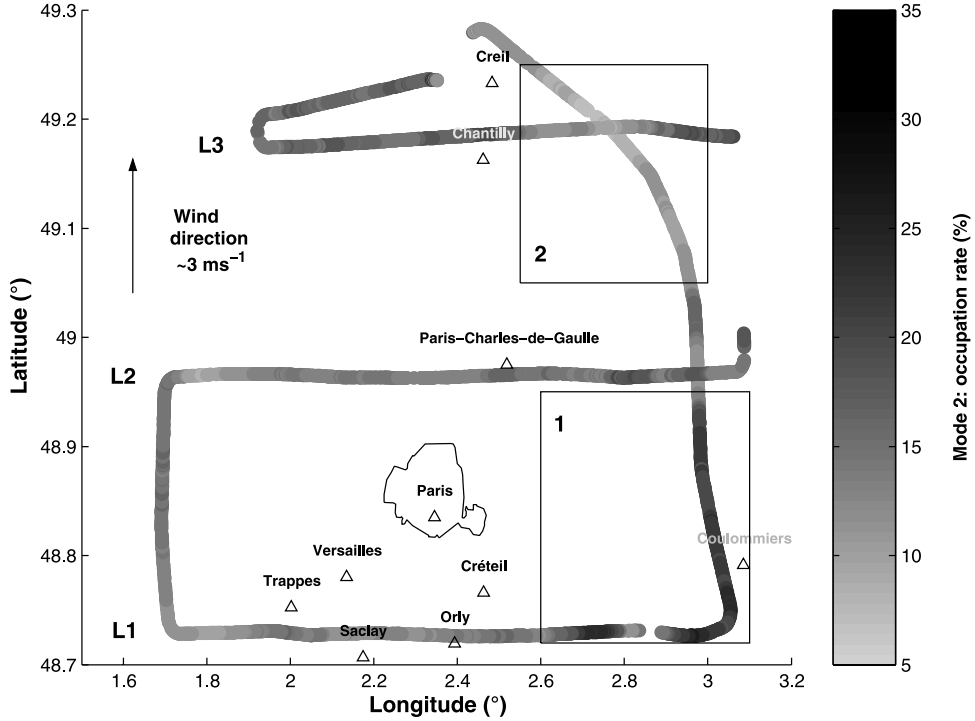

Figure 9. Occupation rate of the second mode (x_2) in the PBL (900 m MSL) along the flight track on 31 July 2000. The domain labeled 1 delimits a region of intensive agricultural activity. The domain labeled 2 corresponds to the area downwind of the Charles de Gaulle Airport influenced by an intense aircraft traffic (see text for details). See color version of this figure at back of this issue.

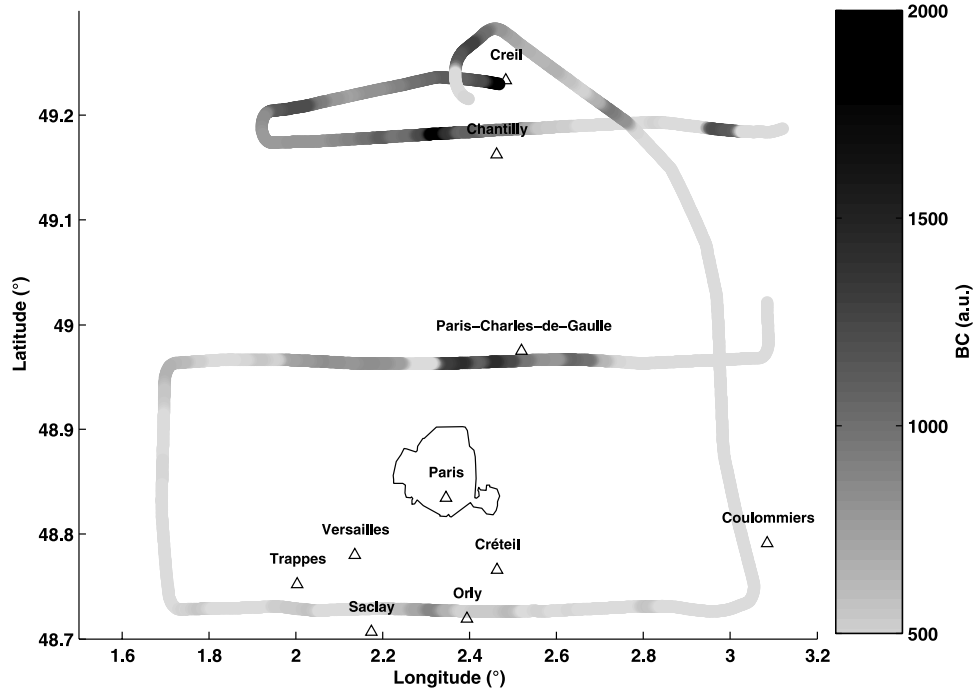

Figure 10. Proxy for the BC concentration (i.e., uncalibrated BC concentration) in the PBL (900 m MSL) along the flight track on 31 July 2000.

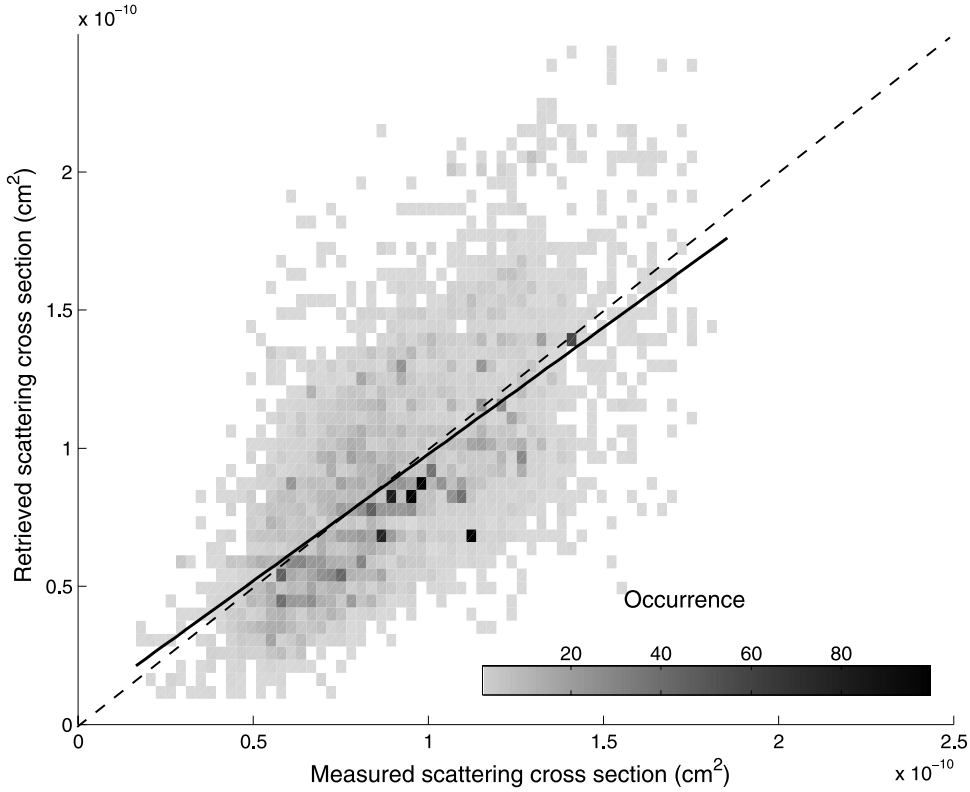

Figure 11. Scatterplot of the retrieved aerosol scattering cross section at 550 nm (computed using Mie theory and the size distributions) against the nephelometer-derived aerosol scattering cross section at 550 nm. All the measurements made on 19 and 31 July 2000 have been considered (~9000 points in the PBL). The dashed line represents the bisectrice. The best fit is given by the thin solid line.

deviations, associated to the mean values, reflect both the temporal variability of the aerosol properties and the error on the retrieved parameters.

[33] The aerosol scattering coefficient at 550 nm in the PBL was computed using Mie theory on the basis of the size distributions determined in section 3.2 and compared to the scattering coefficient measured at 550 nm by the airborne nephelometer during the two days. Since the spectral variability of the continental aerosol refractive index is very weak in the visible domain [*Volz*, 1973], the mean refractive index derived at 670 nm was used. The results, in terms of scattering cross sections, are given in Figure 11 for more than 9000 measurements. They show a good agreement between measurements and simulations with a slope close to 1.05 and a weak bias. The observed dispersion is largely within the quoted refractive index error bars. The uncertainties on the scattering cross section, due to both real and imaginary parts of the refractive index, have been assessed using a Monte Carlo approach [*Chazette et al.*, 2001]. The total relative uncertainty is close to 20% and falls inside the spread shown in Figure 11. Nephelometer measurements are less reliable in case of wet conditions, when the relative humidity (RH) is greater than 50%. On both days, the RH measured at 900 m MSL remained fairly constant during the entire flights, with a mean value of ~60%. The effect on the nephelometers measurements is however expected to be weak, as confirmed by Figure 11.

[34] The single scattering albedo computed at 550 nm exhibits mean values ranging from 0.85 to 0.92 for the mean refractive index here considered. These values are close to the mean AERONET value (0.87 ± 0.068). The uncertainty on the single scattering albedo has been assessed to be close to 0.06 considering the refractive index variation range. Similar single scattering albedo has been retrieved from TARFOX (0.89 to 0.93 [*Russel et al.*, 1999]) and ACE-2 (0.91 to 0.97 [*Carrico et al.*, 2000]) campaigns for pollution outbreaks downwind of the United State East coast and Portugal, respectively. The mean value found during INDOEX was also similar in Goa (0.83 to 0.93 [*Randriamiarisoa et al.*, 2004]) for aerosols resulting from a mixing of biomass and fossil fuel burnings. Moreover, the values retrieved around Berlin in the framework of LACE 98 are similar to our results [*Ansmann et al.*, 2002].

[35] The Angström exponent has been determined from the three-wavelength nephelometer between 450 and 700 nm. The results give a value of 2.1 ± 0.24 for all flights. It is in good agreement with the computed values deduced from the retrieved size number distributions which lead to a mean value of 2.5 ± 0.17. For the latter, an additional uncertainty of 0.06, due to the refractive index, has also been assessed using a Monte Carlo approach. For both results, the given standard deviation, associated to the mean values, reflect the temporal variability of the aerosol properties.

4.2. Coherence With Lidar Measurements

[36] A complementary indirect verification of the coherence between the size number distributions and the optical properties of the aerosol is given by the confrontation of the

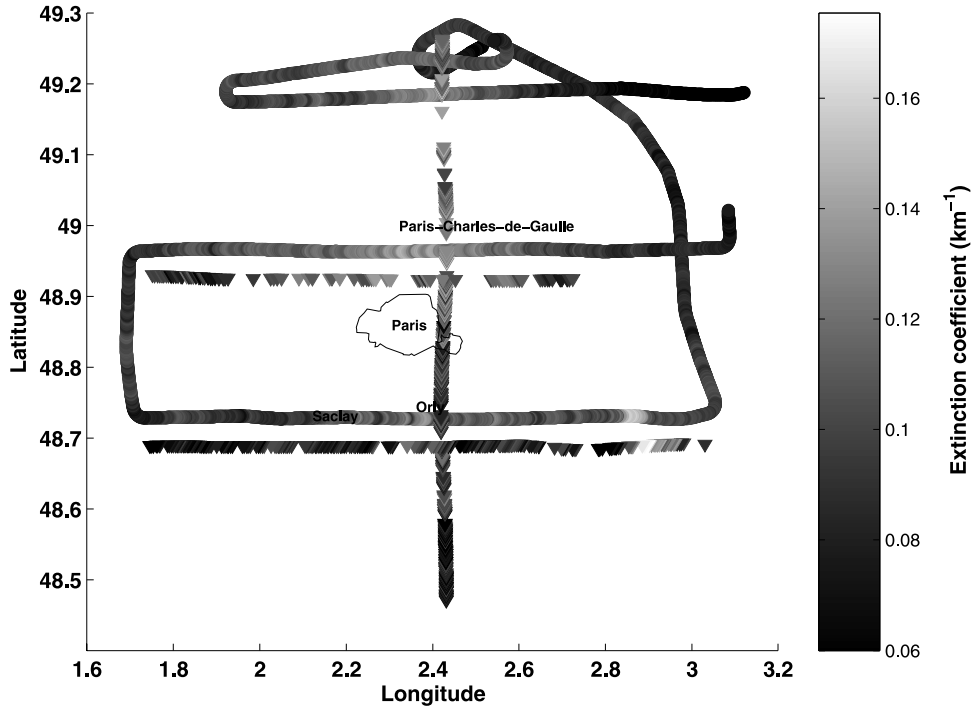

Figure 12. Aerosol extinction coefficients derived from lidar (triangles) and measured in situ by the airborne nephelometer (circles) at ~900 m MSL on 31 July 2000. Legs T1 and T2 (lidar) have been shifted south by 0.04° for the sake of clarity. See color version of this figure at back of this issue.

in situ nephelometer measurements with the lidar extinction retrievals.

[37] The lidar equation has 2 unknowns: the extinction and backscatter coefficients at a given range. Extinction coefficient profiles can be retrieved from raw lidar backscatter profiles (the so-called lidar inversion procedure) provided that assumptions are made on the backscattering-to-extinction ratio (BER) fluctuations with height and if a boundary condition can be determined [e.g., *Klett*, 1981, 1983]. In the present case, the boundary condition was determined by considering the atmosphere to be free of aerosols in a region of the free troposphere (between 3 and 4 km MSL). Exogenous data are needed to determine the BER. The adopted procedure calls on the coupling between coincident measurements of lidar backscattered profiles and aerosol optical thickness determination with photometers. It has been well described in previous works by *Chazette* [2003] for a ground lidar and a ground Sun photometer coupling and by *Pelon et al.* [2002] in similar ground Sun photometer and airborne lidar condition. The inversion is then based on the algorithm proposed by *Klett* [1983].

[38] Coincident lidar and AERONET Sun photometer observations were available above Creil, Paris and Palaiseau (see section 2.3). Their coupling gives access to both the vertical profile of the aerosol extinction coefficient and the BER. The BER values retrieved from profiles at the location of the above mentioned Sun photometers are very similar, ranging from 0.013 to 0.017 sr^{-1}. Calculations performed directly from the experimental aerosol size distributions, through Mie theory, lead to values between 0.013 and 0.018 sr^{-1} and are in good agreement with the previous result. As discussed in section 5, the accumulation mode is the major contributor to the total aerosol extinction coefficient. When only this mode (modal radius of 0.12 μm) is considered, the BER is equal to 0.014 sr^{-1}. We have thus chosen to use this BER value to inverse all the available lidar profiles. Such a value is within the range retrieved in the framework of EARLINET by *Matthias et al.* [2004] (between ~0.013 and ~0.035 sr^{-1}). *Ansmann et al.* [2001] have reported values between 0.017 and 0.035 sr^{-1} for a pollution outbreak from Europe during ACE-2. It thus seems that the values retrieved for Paris aerosol are in the lower limit of all these quoted values.

[39] It is also interesting to compare the aerosol extinction coefficient retrieved from these lidar profiles at an altitude of 900 m MSL with those obtained from the nephelometer measurements. The aerosol extinction coefficient can be calculated from the nephelometer raw scattering coefficient (α_d) measurements, the value of the single scattering albedo $\omega_0 = 0.9$ and the correction factor ξ (see section 2.1.5) as being equal to $\xi\alpha_d/\omega_0$.

[40] The comparison between the two "types" of aerosol extinction coefficients is illustrated in Figure 12 for 31 July data. For locations where both methods can be directly compared, the agreement is very good with a mean difference of 0.01 km^{-1}. Nevertheless, the optical thickness at 532 nm retrieved from lidar in the upwind leg, south of Paris, (0.16) is larger than the one calculated from the Sun photometers at Palaiseau or Creteil (0.11) whereas the coherence is better with the Sun photometer inside Paris (0.15). The observed difference stays within the range of the possible variability of the BER. It must be noted however that the determination of the optical thickness at 532 nm is more questionable when the values are small because the

Table 2. Mean Contribution to the Optical Scattering at 550 nm for Each Mode of the Aerosol Size Distributions Determined From Surface and Airborne Measurements in the PBL

	Mode 1, %	Mode 2, %	Mode 3, %
Airborne measurements			
19 July 2000	14	86	-
31 July 2000	6	94	-
Ground level (MAS)			
19 July 2000 (Saclay)	4	77	19
31 July 2000 (Creil)	5	60	35

Angström exponent derived from the Sun photometer channels then has large uncertainties (more than 30%). The overall coherence of the results presented in this section gives a good confidence level for both retrieved aerosol optical properties and size distributions.

5. Discussion

[41] The contributions of each aerosol mode to the scattering at 550 nm, evaluated from Mie theory with the modal distributions assessed in section 3, are given in Table 2. The second mode with a modal radius of 0.12 μm exhibits the greatest contribution to the total extinction. At the surface, the third mode with a modal radius of ∼0.40 μm plays a non negligible role on the aerosol extinction properties.

[42] The lidar LEANDRE operates at 532 nm and is thus not sensitive to the contribution of the light scattered by aerosols in the nucleation mode. However, it should be sensitive to the light scattered by aerosols in the coarse mode, provided that such aerosols are present in the PBL, above the surface layer. The fact that the extinction coefficients, derived from lidar measurements at 900 m MSL assuming the presence of aerosols in the sole accumulation mode (assumption of a BER = 0.014 sr^{-1}, see section 4.2), are consistent with those retrieved from nephelometer measurements suggests that coarse mode aerosols were not significantly present in the PBL mixed layer, but only within the surface layer. The coherence between the aerosol scattering coefficients calculated from the retrieved size distribution and those measured with the nephelometer leads to the same conclusion.

[43] On 19 July 2000, there is no significant modification of the aerosol extinction coefficient between upwind (north of Paris) and downwind (south of Paris) conditions, as illustrated in the Figure 13, where similar lidar profiles (averaged over legs T1 and T2, respectively) are observed. The presence of a residual aerosol layer is highlighted between 1.5 and 2.5 km MSL. The lidar-derived aerosol optical thickness variation between the north and the south is within the uncertainty range associated with the lidar inversion procedure. The same observation can be made from the nephelometer raw scattering coefficient with mean values of 0.15 ± 0.01 km^{-1} for the upwind leg L1 and 0.14 ± 0.01 km^{-1} for the downwind legs L2 and L3 (Figure 2a). The corresponding aerosol number concentration measured by the airborne CPC increased from 4600 ± 1500 on leg L1 to 7200 ± 1900 cm^{-3} on legs L2 and L3. Hence it appears that the city of Paris mainly produces aerosols in the nucleation mode (modal radius of ∼0.03 μm) that have almost no influence on the aerosol optical properties at 550 nm. The fact that the aerosol optical properties do not evolve between the north and south of Paris suggests that the accumulation mode (modal radius of ∼0.12 μm) already dominates the aerosol size distribution in the incoming air mass, as it could be expected for an atmospheric flow polluted by aerosols having aged for several days.

[44] Depending on the nature of the aerosols, the lidar signal (besides being sensitive to aerosol number concentration) can be sensitive to relative humidity in the PBL. In

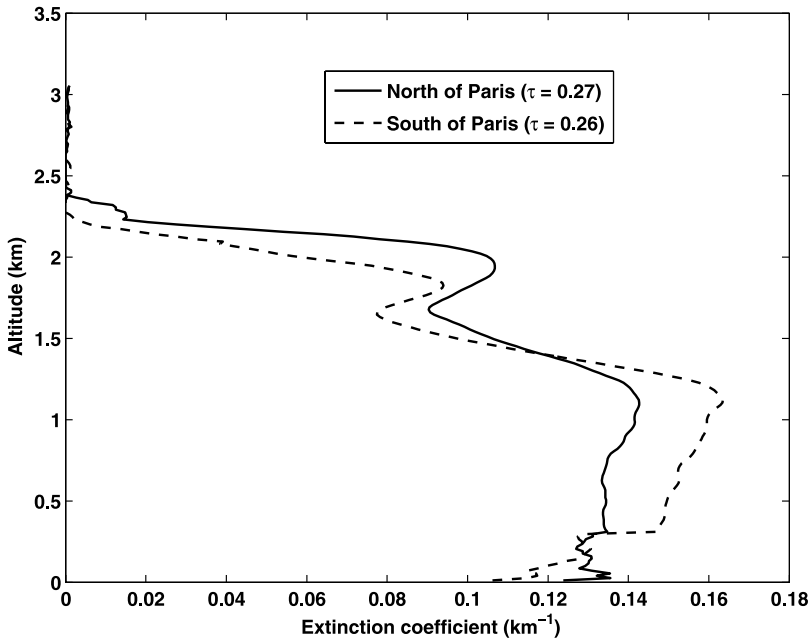

Figure 13. Mean profile of the aerosol extinction coefficient obtained by lidar north (upwind) and south (downwind) of Paris on legs T1 and T2, respectively, on 19 July 2000.

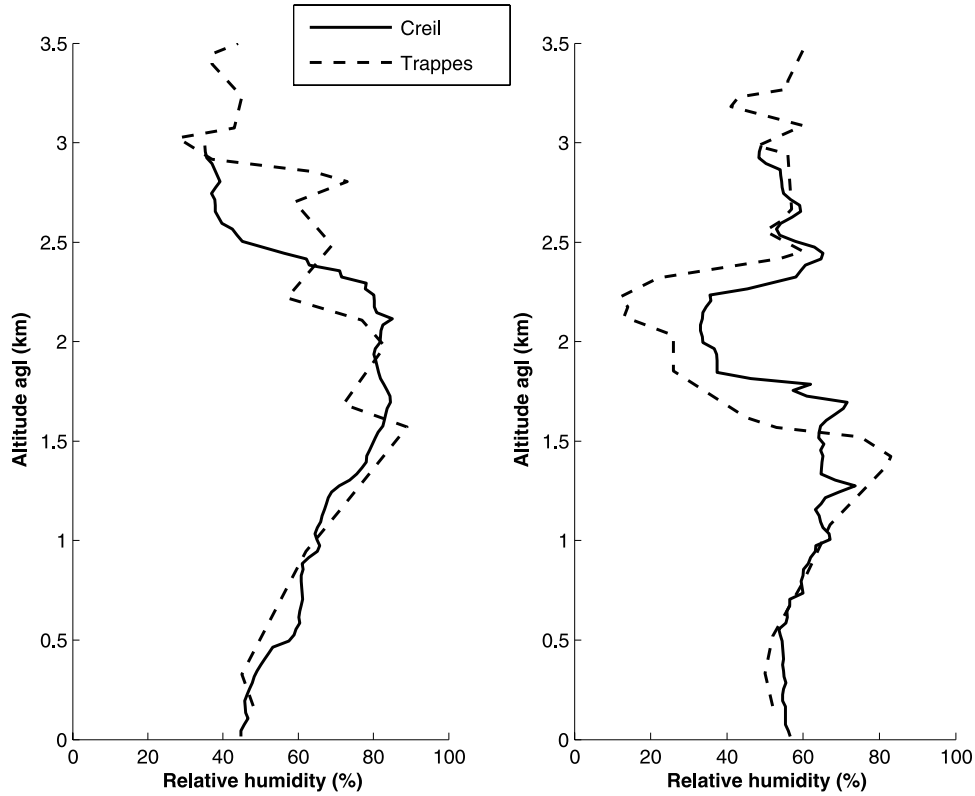

Figure 14. Relative humidity profiles on (left) 19 July and (right) 31 July acquired by the ARAT in the vicinity of Creil shortly before landing (solid lines) and obtained from a balloon sounding in Trappes (dashed lines). The airborne profiles were obtained around 1700 and 1400 UTC on 19 and 31 July, respectively. The soundings in Trappes were performed at 1200 UTC.

Figure 14 we have compared the RH profiles obtained north of Paris (by aircraft) and southwest of Paris (balloon soundings at Trappes) and found that RH profiles were very similar on both sides of Paris (as also suggested by the aircraft measurements in the PBL, at 900 m MSL). RH profiles were found to increase from 45% at the surface to 75% at the top of the PBL. The fact that the lidar-derived extinction profile remained more or less constant in the PBL could be an indication that for 19 July the aerosols in the accumulation mode were essentially hydrophobic.

[45] On 31 July 2000 the situation is quite different, as shown in Figure 15. The aerosol extinction coefficient determined from lidar profiles increased significantly in the entire PBL between upwind leg T1 (south) and downwind leg T2 (north). The influence of the RH profile on the aerosol optical properties is clearly visible for 31 July, in Figure 15. The two-dimensional lidar-derived aerosol extinction coefficients shown in Figure 16 highlight an increase of the aerosol optical extinction between the southern and the northern parts of the Paris area. The optical thickness at 532 nm evolved from 0.12 at ~45 km south of Paris, over the countryside, to 0.16 over Orly, 15 km south of Paris, up to 0.26 over Creil, 40 km north of Paris. Figure 16 also shows that the PBL depth increased slightly with latitude. Within the pollution plume the nephelometer raw scattering coefficient (Figure 2b) increased from 0.08 ± 0.01 km^{-1} (upwind, leg L1) to 0.12 ± 0.01 km^{-1} (downwind, leg L2) at the altitude of ~900 m MSL. The simultaneous CPC measurements show a mean number aerosol concentration increase from 7300 ± 2300 upwind to 9700 ± 2000 cm^{-3} downwind. As indicated in section 2.2, leg L1 was flown over a rather urbanized area and the above upwind mean aerosol number concentration is most likely not representative of the aerosol loading in the maritime incoming air mass. Nevertheless, the increase in the lidar derived extinction coefficients in the PBL suggests, for a given altitude level, an increase in number concentration of aerosols in the accumulation mode. It is not believed that this increase on the lidar signal is fully proportional to aerosol production by Paris. Rather, the incoming clean air mass is contaminated by pollution upon arrival over the Paris area and fast aerosol aging processes are being observed more distinctly than in the 19 July case. We have also compared the RH profiles obtained upwind (by aircraft) and downwind (Trappes balloon soundings) and found that RH profiles were very similar on both sides of Paris (Figure 14). RH profiles were found to increase from 55% at the surface to 80% at the top of the PBL. The sharp maximum observed on the aerosol extinction coefficient at the top of the PBL for 31 July (Figure 15) is linked to aerosol size growth with increasing RH [*Hänel*, 1976], suggesting that these aerosols in the accumulation mode are hydrophilic. Hence in situ measurements of the aerosol properties retrieved at 900 m MSL are not representative for the entire PBL.

[46] Finally, in the region influenced by the Charles de Gaulle Airport (domain 2 in Figure 9), and located outside the Paris pollution plume, a significant amount of particles

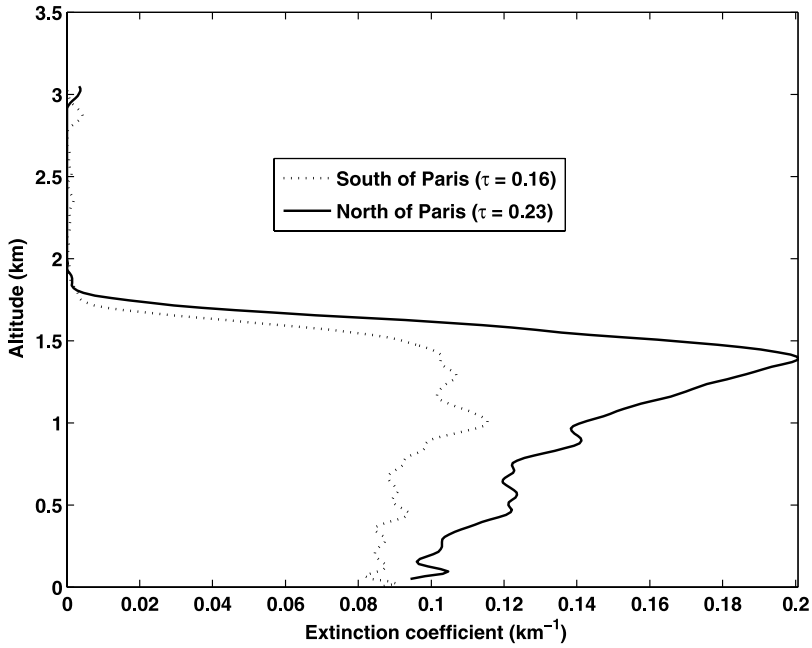

Figure 15. Mean profile of the aerosol extinction coefficient obtained by lidar south (upwind) and north (downwind) of Paris on legs T1 and T2, respectively, on 31 July 2000.

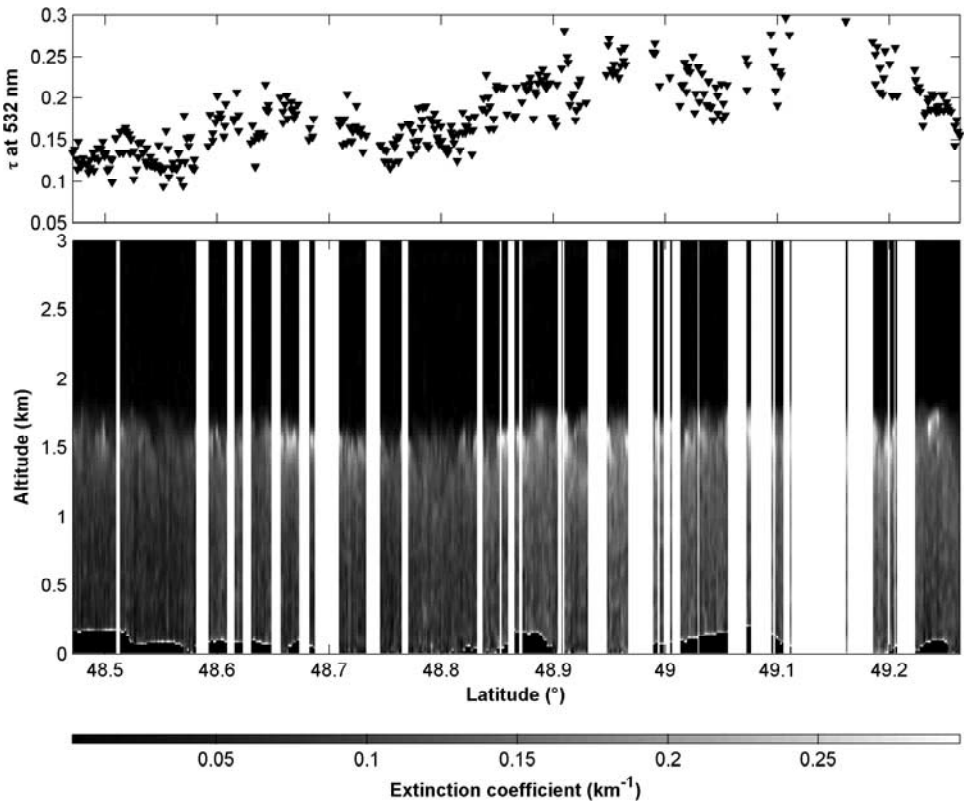

Figure 16. (top) Lidar-derived aerosol optical thickness at 532 nm and (bottom) vertical profile of the extinction coefficient obtained along leg T3 (oriented south-north) by LEANDRE on 31 July. The vertical white stripes correspond to missing data due to contamination by cumulus clouds present at the top of the PBL. See color version of this figure at back of this issue.

were observed to be produced (the airborne CPC measured total concentrations higher than 10^4 cm^{-3} at 900 m MSL) even though they barely contributed to the overall aerosol optical properties in the visible spectral range. As shown in Figure 12, the aerosol extinction coefficient is $\sim$0.06 km^{-1} in this area, compared to $\sim$0.12 km^{-1} within the Paris plume. The occupation rate of the second mode has been established to be as low as $\sim$12% in this region (see Table 1 and Figure 9), indicating a strong proportion of small particles, probably directly produced within the PBL by intense aircraft traffic.

6. Conclusion

[47] For the first time airborne measurements were performed above the Paris area to study the anthropogenic aerosols in the mixed layer. Authorizations were obtained for flights at two levels, the first for in situ measurements, close to 900 m MSL, and the second around 4200 m MSL for lidar measurements. Two well-defined pollution plumes were sampled for representative air mass origins. The 19 July (31 July) event was characterized by north-northwesterly (westerly) advection of polluted (clean) air masses originating from Great Britain (the Atlantic Ocean). On both days, the aerosol number size distribution was composed of two modes in the planetary boundary mixed layer (accumulation and nucleation) and three modes in the surface layer (accumulation, nucleation, and coarse). The characteristics of the size distribution (modal radii, geometric dispersion) were remarkably similar on both days.

[48] An original combination of airborne backscatter lidar and in situ (nephelometer, particle sizer) measurements evidenced that the city of Paris mainly produces aerosols in the nucleation mode (modal radius of $\sim$0.03 μm) that have almost no influence on the aerosol optical properties in the visible spectral range. Emissions are mainly due to automobile and aircraft traffic [*Menut*, 2003]. The aerosol optical properties at 550 nm were dominated by the scattering properties of aerosols in the accumulation mode (for $\sim$90% on average). Lidar measurements from the airborne LEANDRE-1 system show that the aerosol production of Paris impacts on the entire PBL. Relative humidity effects are far from being negligible on pollution aerosols produced by the Paris area. Nevertheless, if they are clearly observed on ''young'' hydrophilic aerosols in the accumulation mode, they appear relatively weaker when polluted air masses arrive over Paris loaded with aged, hydrophobic particles, coming from Great Britain.

[49] This experiment demonstrates the complementarity between in situ sampling analysis and active remote sensing measurements to study aerosols in the lower and middle troposphere. Such an approach will be used in the framework of future international campaigns such as the African Monsoon Multidisciplinary Analyses (AMMA, http://amma.africa-web.org/) experiment during which airborne measurements will take an important place.

[50] Moreover, our results from airborne lidar measurements stress the sensitivity of lidar backscattered signals and their usefulness in analyzing regional pollution transport processes. The arrival of a new generation of space-borne instruments such as the lidar system CALIOP on CALIPSO (http://www-calipso.larc.nasa.gov/) to be launched at the beginning of 2005 should thus offer new perspectives for aerosol pollution studies.

[51] **Acknowledgments.** This work was supported by the Programme National de Chimie Atmosphérique, the Institut National des Sciences de l'Univers (INSU) and the Commissariat à l'Energie Atomique. The authors would like to thank Guy Penazzi and André Gribkoff from the Division Technique of INSU as well as Jacques Pelon and Michael Sicard from the Service d'Aéronomie. AIRPARIF is also acknowledged for providing its ground station data. Bernadette Chatenet is acknowledged for helping with the Sun photometer measurements in the framework of the AERONET network. The authors thank Elizabeth Devlin for her careful reading of the manuscript. This is LSCE contribution number 1331.

References

Ansmann, A., F. Wagner, D. Althausen, D. Müller, A. Herber, and U. Wandinger (2001), European pollution outbreaks during ACE-2: Lofted aerosol plumes observed with Raman lidar at the Portuguese coast, *J. Geophys. Res.*, *106*, 20,725–20,733.

Ansmann, A., U. Wandinger, A. Wiedensohler, and U. Leiterer (2002), Lindenberg aerosol characterization experiment 1998 (LACE 98): Overview, *J. Geophys. Res.*, *107*(D21), 8129, doi:10.1029/2000JD000233.

Barker, J., and D. T. Tingey (1992), *Air Pollution Effects on Biodiversity*, 304 pp., Springer, New York.

Beekmann, M., and C. Derognat (2003), Monte Carlo uncertainty analysis of a regional-scale transport chemistry model constrained by measurements from the Atmospheric Pollution Over the Paris Area (ESQUIF) campaign, *J. Geophys. Res.*, *108*(D17), 8559, doi:10.1029/2003JD003391.

Bennet, B. G., J. G. Kretzchmar, G. G. Akland, and H. W. Koning (1985), Urban air pollution worldwide, *Environ. Sci. Technol.*, *19*, 298–304.

Bodhaine, B. A., N. C. Ahlquist, and R. C. Schnell (1991), Three-wavelength nephelometer suitable for aircraft measurements of background aerosol scattering coefficient, *Atmos. Environ.*, *10*, 2268–2276.

Carrico, C. M., M. J. Rood, J. A. Ogren, C. Neusüß, A. Wiedensohler, and J. Heintzenberg (2000), Aerosol optical properties at Sagres, Portugal during ACE 2, *Tellus, Ser. B*, *52*, 694–715.

Chazette, P. (2003), The monsoon aerosol extinction properties at Goa during INDOEX as measured with lidar, *J. Geophys. Res.*, *108*(D6), 4187, doi:10.1029/2002JD002074.

Chazette, P., and C. Liousse (2001), A case study of optical and chemical ground apportionment for urban aerosols in Thessaloniki, *Atmos. Environ.*, *35*(14), 2497–2506.

Chazette, P., C. David, J. Lefrère, S. Godin, J. Pelon, and G. Mégie (1995), Comparative lidar study of the optical, geometrical, and dynamical properties of stratospheric post-volcanic aerosols, following the eruption of El Chichon and Mount Pinatubo, *J. Geophys. Res.*, *100*, 23,195–23,207.

Chazette, P., G. Mégie, and J. Pelon (1998), Potential use of spaceborne lidar measurements to improve atmospheric temperature retrievals from passive sensors, *Appl. Opt.*, *37*, 7670–7679.

Chazette, P., J. Pelon, and G. Mégie (2001), Determination by spaceborne backscatter lidar of the structural parameters of atmospheric scattering layer, *App. Opt.*, *40*, 3428–3440.

Chedin, A., and N. A. Scott (1985), Initialization of the radiative transfer equation problem from a pattern recognition type approach: Application to the satellites of the TIROS-N series, in *Advances in Remote Sensing Retrieval Methods*, edited by A. Deepak, H. E. Fleming, and M. T. Chahine, pp. 495–515, A. Deepak, Hampton, Va.

Cutten, D. R., J. D. Spinhirne, R. T. Menzies, D. A. Bowdle, V. Srivastava, R. F. Pueschel, A. D. Clarke, and J. Rothermel (1998), Intercomparison of pulsed lidar data with flight level CW lidar data and modeled backscatter from measured aerosol microphysics near Japan and Hawaii, *J. Geophys. Res.*, *103*, 19,649–19,661.

Derognat, C., M. Beekmann, M. Baeumle, D. Martin, and H. Schmidt (2003), Effect of biogenic volatile organic compound emissions on tropospheric chemistry during the Atmospheric Pollution Over the Paris Area (ESQUIF) campaign in the Ile-de-France region, *J. Geophys. Res.*, *108*(D17), 8560, doi:10.1029/2001JD001421.

Dickerson, R. R., S. Kondragunta, G. Stenchikov, K. L. Civerolo, B. G. Doddrige, and B. N. Holben (1997), The impact of aerosols on solar ultraviolet radiation and photochemical smog, *Science*, *278*, 827–830.

Draxler, R. R., and G. D. Hess (1998), An overview of the Hysplit_4 modeling system for trajectories, dispersion, and deposition, *Aust. Meteorol. Mag.*, *47*, 295–308.

Dubovik, O., B. N. Holben, T. F. Eck, A. Smirnov, Y. J. Kaufman, M. D. King, D. Tanré, and I. Slutsker (2001), Variability of absorption and optical properties of key aerosol types observed in worldwide locations, *J. Atmos. Sci.*, *59*, 590–608.

Durieux, E., L. Fiorani, B. Calpini, M. Flamm, L. Jaquet, and H. Van der Bergh (1998), Tropospheric ozone measurements over the greater Athens area during the MEDCAPHOT-TRACE campaign in Athens, Greece (20 August–20 September), *Atmos. Environ.*, 2141–2150.

Dye, J. E., and D. Baumgardner (1984), Evaluation of the forward scattering spectrometer probe: I. Electronic and optical studies, *J. Atmos. Ocean. Technol.*, *1*, 329–344.

Eleftheriadis, K., D. Balis, I. Colbeck, and N. Manalis (1998), Atmospheric aerosol and gaseous species in Athens, Greece, *Atmos. Environ.*, *32*, 2183–2191.

Flamant, C., and J. Pelon (1996), Atmospheric boundary-layer structure over the Mediterranean during a Tramontane event, *Q. J. R. Meteorol. Soc.*, *122*, 1741–1778.

Flamant, C., et al. (2000), Airborne lidar measurements of aerosol spatial distribution and optical properties over the Atlantic Ocean during a European pollution outbreak of ACE-2, *Tellus, Ser. B*, *52*, 662–677.

Forstner, H. J. L., J. H. Seinfeld, and R. C. Flagan (1997), Secondary organic aerosol formation from the photooxidation of aromatic hydrocarbons. Molecular composition, *Environ. Sci. Technol.*, *31*, 1345–1358.

Hamonou, E., P. Chazette, D. Balis, F. Dulac, X. Schneider, E. Galani, G. Ancellet, and A. Papayannis (1999), Characterization of the vertical structure of Saharan dust export to the Mediterranean basin, *J. Geophys. Res.*, *104*, 22,257–22,270.

Hänel, G. (1976), The properties of atmospheric aerosol particles as functions of the relative humidity at thermodynamic equilibrium with the surrounding moist air, *Adv. Geophys.*, *19*, 73–188.

Hansen, A. D. A., and T. Novakov (1990), Real time measurements of aerosol black carbon during the carbonaceous species methods comparison study, *Aerosol Sci. Technol.*, *12*, 194–199.

Harrison, R. M., and J. Yin (2000), Particulate matter in the atmosphere: Which particle properties are important for its effects on health?, *Sci. Total Environ.*, *249*, 85–101.

Holben, B. N., et al. (1998), AERONET—A federated instrument network and data archive for aerosol characterisation, *Remote Sens. Environ.*, *66*, 1–16.

Intergovernmental Panel on Climate Control (IPCC) (2001), *Climate Change 2001, the Third Assessment Report of the IPCC*, Cambridge Univ. Press, New York.

Jones, A. P. (1999), Indoor air quality and health, *Atoms. Environ.*, *33*, 4535–4564.

Klett, J. D. (1981), Stable analytical inversion solution for processing lidar returns, *Appl. Opt.*, *20*, 211–220.

Klett, J. D. (1983), Lidar inversion with variable backscatter/extinction ratios, *Appl. Opt.*, *24*, 1638–1643.

Léon, J. F., P. Chazette, J. Pelon, F. Dulac, and H. Ramdriamarisoa (2002), Aerosol direct radiative impact over the INDOEX area based on passive and active remote sensing, *J. Geophys. Res.*, *107*(D19), 8006, doi:10.1029/2000JD000116.

Lurmann, F. W., A. S. Wexler, S. N. Pandis, S. Musarra, N. Kumar, and J. H. Seinfeld (1997), Modeling urban and regional aerosols: II. Application to California's South coast air basin, *Atmos. Environ.*, *31*, 2695–2715.

Matthias, V., et al. (2004), Aerosol lidar comparison in the framework of the EARLINET project. 1. Instruments, *Appl. Opt.*, *43*, 961–976.

Menut, L. (2003), Adjoint modeling for atmospheric pollution process sensitivity at regional scale, *J. Geophys. Res.*, *108*(D17), 8562, doi:10.1029/2002JD002549.

Menut, L., et al. (2000), Measurements and modeling of atmospheric pollution over the Paris area: An overview of the ESQUIF project, *Ann. Geophys.*, *18*(11), 1467–1481.

Pelon, J., C. Flamant, P. Chazette, J. F. Leon, D. Tanré, M. Sicard, and S. K. Satheesh (2002), Characterization of aerosol spatial distribution and optical properties over the Indian Ocean from airborne lidar and radiometry during INDOEX'99, *J. Geophys. Res.*, *107*(D19), 8029, doi:10.1029/2001JD000402.

Pena, J. A., J. M. Norman, and D. W. Thomson (1977), Isokinetic sampler for continuous airborne aerosol measurements, *J. Air Pollut. Control Assoc.*, *27*(4), 337–3341.

Penner, J. E. (1995), Carbonaceous aerosols influencing atmospheric radiation: Black and organic carbon, in *Report of the Dahlem Workshop on Aerosol Forcing of Climate*, edited by R. J. Charlson and J. Heintzenberg, pp. 91–108, John Wiley, Hoboken, N. J.

Randriamiarisoa, H., P. Chazette, and G. Mégie (2004), The columnar retrieved single scattering albedo from NO_2 photolysis rate, *Tellus, Ser. B*, *56*, 118–127.

Ramanathan, V., et al. (2001), The Indian Ocean Experiment: An integrated assessment of the climate forcing and effects of the great Indo-Asian haze, *J. Geophys. Res.*, *106*, 28,371–28,393.

Russel, P. B., J. M. Livingston, P. Hignett, S. Kinne, J. Wong, A. Chien, R. Bergstoom, P. Durkee, and P. V. Hobbs (1999), Aerosol-induced radiative flux change off the United States mid-Atlantic coast: Comparison of values calculated from sunphotometer and in situ data with those measured by airborne pyranometer, *J. Geophys. Res.*, *104*, 2289–2307.

Sheridan, P. J., A. Jefferson, and J. A. Ogren (2002), Spatial variability of submicrometer aerosol radiative properties over the Indian Ocean during INDOEX, *J. Geophys. Res.*, *107*(D19), 8011, doi:10.1029/2000JD000166.

Vautard, R., M. Beekmann, J. Roux, and D. Gombert (2001), Validation of a deterministic forecasting system for the ozone concentrations over the Paris area, *Atmos. Environ.*, *35*, 2449–2461.

Vautard, R., et al. (2003a), A synthesis of the Air Pollution Over the Paris Region (ESQUIF) field campaign, *J. Geophys. Res.*, *108*(D17), 8558, doi:10.1029/2003JD003380.

Vautard, R., et al. (2003b), Paris emission inventory diagnostics from ESQUIF airborne measurements and a chemistry transport model, *J. Geophys. Res.*, *108*(D17), 8564, doi:10.1029/2002JD002797.

Volz, F. E. (1973), Infrared optical constants of ammonium sulphate, Saharan dust, volcanic pumice and fly-ash, *Appl. Opt.*, *12*, 564–568.

P. Chazette, P. Couvert, H. Randriamiarisoa, and J. Sanak, Laboratoire des Sciences du Climat et de l'Environnement, Institut Pierre-Simon Laplace, Commissariat à l'Energie Atomique, Centre National de la Recherche Scientifique, Centre d'Etude de Saclay, Bat. 701, F-91191 Gif-sur-Yvette cedex, France. (patrick.chazette@cea.fr)

C. Flamant, Service d'Aéronomie, Institut Pierre-Simon Laplace, Université Pierre et Marie Curie, BP 102, F-75252 Paris Cedex 05, France.

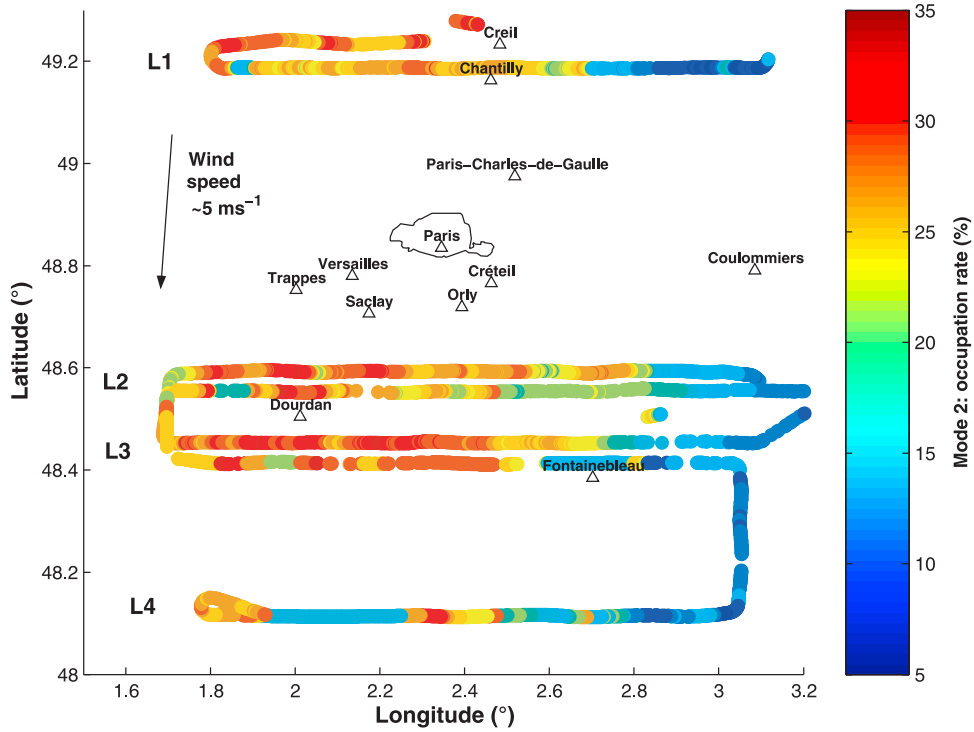

Figure 7. Occupation rate of the second mode (x_2) in the PBL (900 m MSL) along the flight track on 19 July 2000. Legs L2 and L3 for the second flight have been shifted north by 0.04° for the sake of clarity.

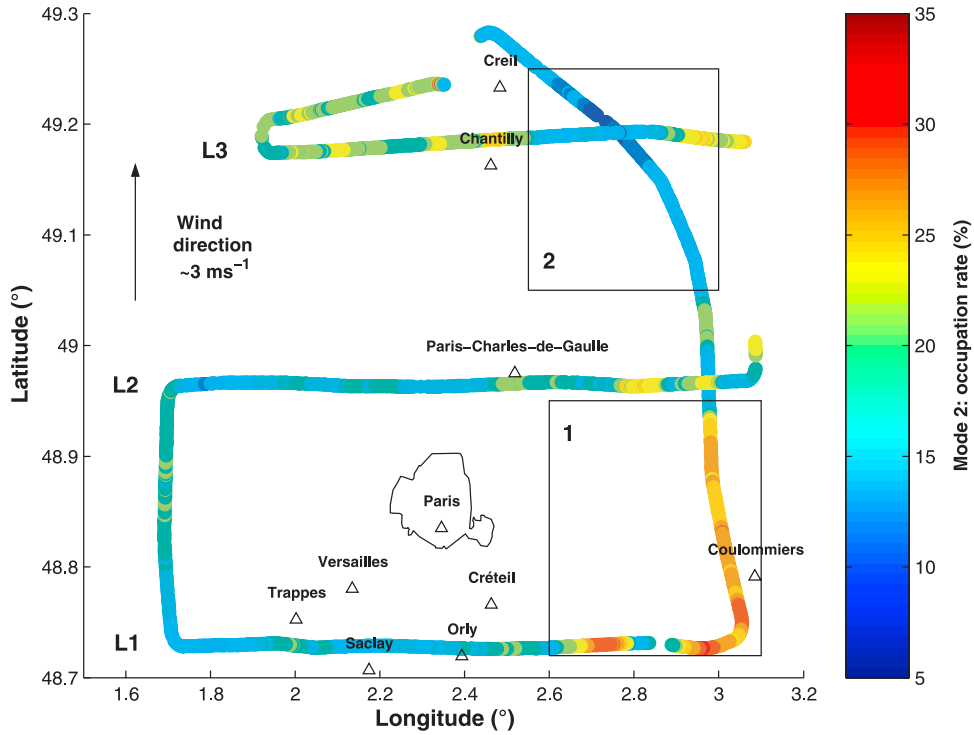

Figure 9. Occupation rate of the second mode (x_2) in the PBL (900 m MSL) along the flight track on 31 July 2000. The domain labeled 1 delimits a region of intensive agricultural activity. The domain labeled 2 corresponds to the area downwind of the Charles de Gaulle Airport influenced by an intense aircraft traffic (see text for details).

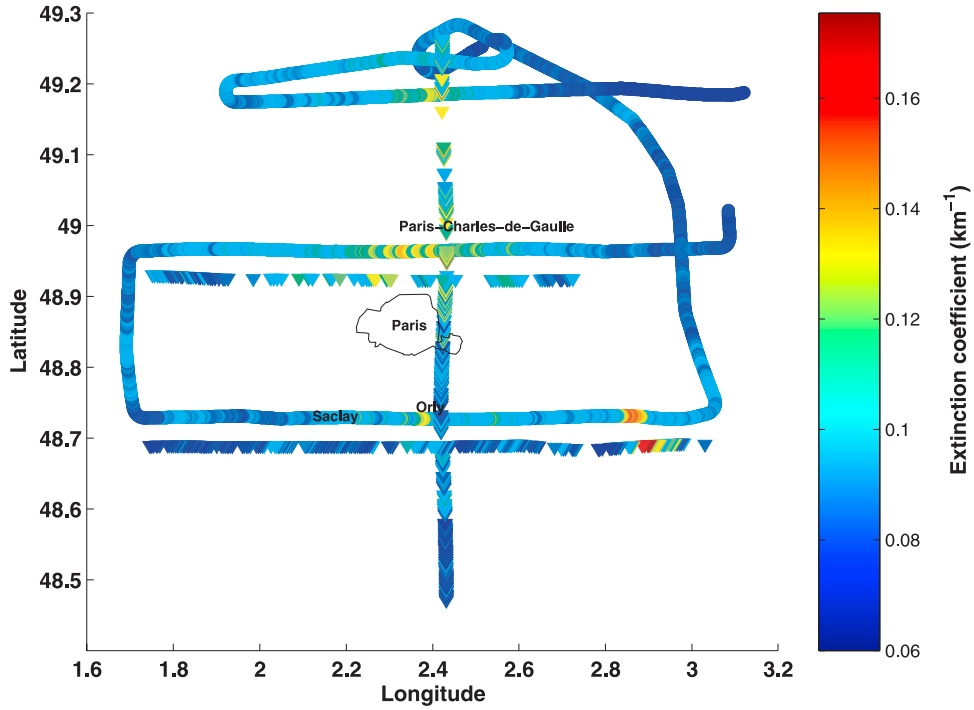

Figure 12. Aerosol extinction coefficients derived from lidar (triangles) and measured in situ by the airborne nephelometer (circles) at ~900 m MSL on 31 July 2000. Legs T1 and T2 (lidar) have been shifted south by 0.04° for the sake of clarity.

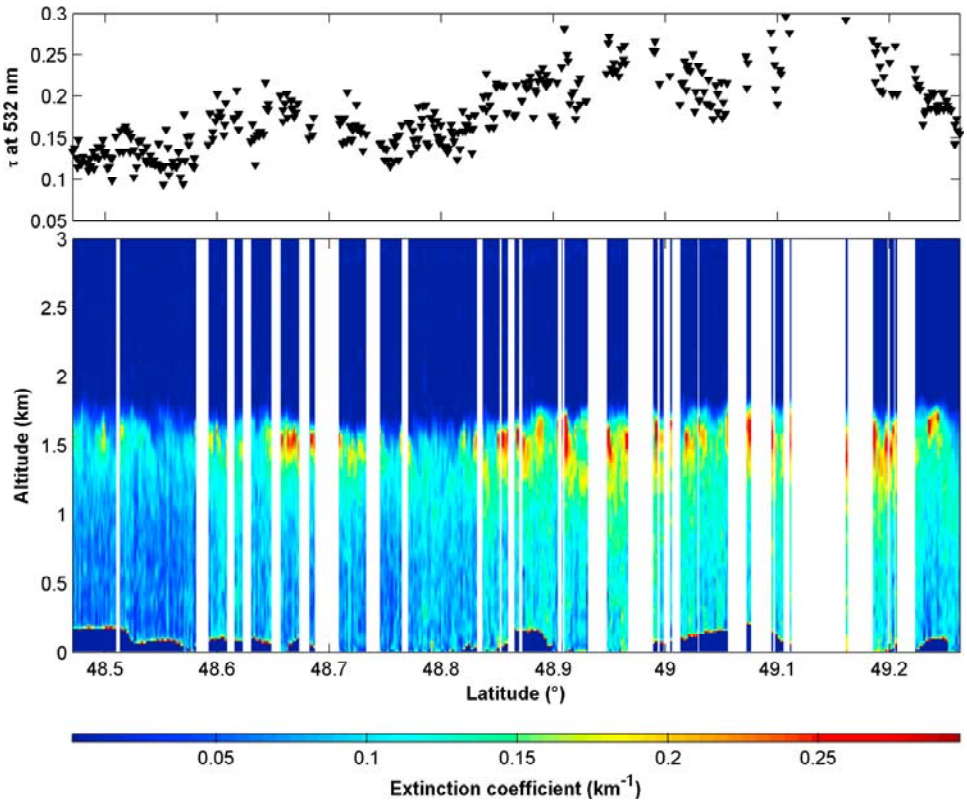

Figure 16. (top) Lidar-derived aerosol optical thickness at 532 nm and (bottom) vertical profile of the extinction coefficient obtained along leg T3 (oriented south-north) by LEANDRE on 31 July. The vertical white stripes correspond to missing data due to contamination by cumulus clouds present at the top of the PBL.